High-Fidelity Hot Gates for Generic Spin-Resonator Systems

M. J. A. Schuetz,[1] G. Giedke,[2,3] L. M. K. Vandersypen,[4] and J. I. Cirac[1]

[1]*Max-Planck-Institut für Quantenoptik, Hans-Kopfermann-Str. 1, 85748 Garching, Germany*
[2]*Donostia International Physics Center, Paseo Manuel de Lardizabal 4, E-20018 San Sebastián, Spain*
[3]*Ikerbasque Foundation for Science, Maria Diaz de Haro 3, E-48013 Bilbao, Spain and*
[4]*Kavli Institute of NanoScience, TU Delft, P.O. Box 5046, 2600 GA Delft, The Netherlands*
(Dated: July 7, 2016)

We propose and analyze a high-fidelity hot gate for generic spin-resonator systems which allows for coherent spin-spin coupling, in the presence of a thermally populated resonator mode. Our scheme is non-perturbative, applies to a broad class of physical systems, including for example spins coupled to circuit-QED and surface acoustic wave resonators as well as nanomechanical oscillators, and can be implemented readily with state-of-the-art experimental setups. We provide and numerically verify simple expressions for the fidelity of creating maximally entangled states under realistic conditions.

Motivation.—The physical realization of a large-scale quantum information processing (QIP) architecture constitutes a fascinating problem at the interface between fundamental science and engineering [1, 2]. With single-qubit control steadily improving in various physical setups, further advances towards this goal currently hinge upon realizing *long-range* coupling between the logical qubits, since coherent interactions at a distance do not only relax some serious architectural challenges [3], but also allow for applications in quantum communication, distributed quantum computing and some of the highest tolerances in error-correcting codes based on long-distance entanglement links [2, 4, 5]. One particularly prominent approach to address this problem is to interface qubits with a common quantum bus which effectively mediates long-range interactions between distant qubits, as has been demonstrated successfully for superconducting qubits [6, 7] and trapped ions [8].

Executive summary.—In the spirit of the celebrated Sørensen-Mølmer or similar gates for *hot* trapped ions [9–20], here we propose and analyze a generic bus-based quantum gate between distant (solid-state) qubits which allows for coherent spin-spin coupling, even in the presence of a thermally populated resonator mode. Our scheme does not rely on a perturbative treatment, but is rather stroboscopic in nature; thus, for certain times the qubits entirely disentangle from the (thermally populated) resonator mode, providing a gate that is insensitive to the state of the resonator and therefore does not require ground-state cooling of the resonator mode. As a consequence, our scheme may provide a potential solution to the solid-state QIP interconnect problem between the quantum (for encoding quantum information) and the classical layer (for classical control and read-out) [21], since it allows operating and coupling qubits at elevated temperatures $\sim (1-4)\,\mathrm{K}$ (as opposed to milli-Kelvin temperatures), so that the qubit plane may be integrated right next to the classical cryogenic electronics. Since we consider a very generic spin-resonator system, our approach is accessible to a broad class of physical systems [22], including for example circuit QED setups

with both (i) superconducting qubits [6, 23, 24], and (ii) spin qubits [25–42], (iii) spins coupled to surface acoustic wave (SAW) resonators [43–45], and (iv) spins coupled to nanomechanical oscillators [46–50]; compare Fig. 1. We discuss in detail the dominant sources of errors for our protocol, due to rethermalization of the resonator mode and qubit dephasing, and numerically verify the expected error scaling.

Analytical model: Hot gate.—We consider a set of spins (qubits) $i = 1, 2, \ldots$ with transition frequencies ω_q coupled to a common (bosonic) cavity mode of frequency ω_c, as described by the Hamiltonian ($\hbar = 1$)

$$H = \omega_c a^\dagger a + \frac{\omega_q}{2} S^z + g\mathcal{S} \otimes \left(a + a^\dagger\right), \qquad (1)$$

$$\mathcal{S} = \sum_{i,\alpha} \eta_i^\alpha \sigma_i^\alpha, \qquad (2)$$

where $\vec{\sigma}_i$ refer to the usual Pauli matrices describing the qubits, $S^z = \sum_i \sigma_i^z$ and a is the bosonic annihilation operator for the resonator mode. The operator $\mathcal{S}$ is a generalized (collective) spin operator which accounts for both transversal ($\alpha = x, y$) and longitudinal ($\alpha = z$) spin-resonator coupling; the unit-less parameters η_i^α capture potential anisotropies and inhomogeneities in the single-photon/phonon coupling constants $g_i^\alpha = \eta_i^\alpha g$.
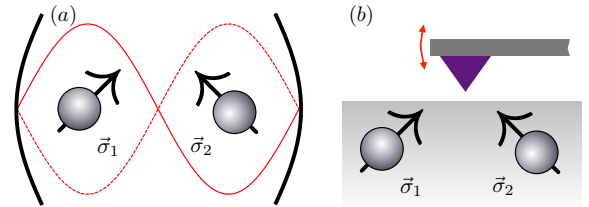

Figure 1: (color online). Schematic illustration for a generic spin-resonator system, comprising a set of spins $\{\vec{\sigma}_i\}$ coupled to a common resonator mode with a non-vanishing thermal occupation. Exemplary candidate spin-resonator systems for such a system include (for example) (a) spins coupled to transmission line [28] or SAW resonators [43], and (b) spins coupled to nanomechanical oscillators [47].

Typically, for artificial atoms such as quantum dots the qubit transition frequencies ω_q are highly tunable. In what follows, we consider the regime where ω_q is much smaller than all other energy scales; therefore, for the purpose of our analytical derivation, effectively we take $\omega_q = 0$. The robustness of our scheme against non-zero splittings ($\omega_q > 0$) will be discussed below. In this limit, the Hamiltonian given in Eq.(1) can be rewritten as

$$H = \omega_c \left(a + \frac{g}{\omega_c}\mathcal{S} \right)^\dagger \left(a + \frac{g}{\omega_c}\mathcal{S} \right) - \frac{g^2}{\omega_c}\mathcal{S}^2, \qquad (3)$$

which comprises a displacement of the cavity mode a by $(g/\omega_c)\mathcal{S}$. Using the relation $UaU^\dagger = a + (g/\omega_c)\mathcal{S}$, with the unitary (polaron) transformation $U = \exp\left[g/\omega_c \mathcal{S} \left(a - a^\dagger \right) \right]$, Eq.(1) can be recast into the form

$$H = U \underbrace{\left[\omega_c a^\dagger a - \frac{g^2}{\omega_c}\mathcal{S}^2 \right]}_{H_0} U^\dagger, \qquad (4)$$

where we have used that $\mathcal{S}$ commutes with U. Now, let us consider the time-evolution governed by the Hamiltonian H. It reads

$$e^{-iHt} = e^{-iUH_0U^\dagger t} = U e^{-i\omega_c t a^\dagger a} e^{i\frac{g^2}{\omega_c}t\mathcal{S}^2} U^\dagger, \qquad (5)$$

where the second equality directly follows from $\exp(x) = \sum_n x^n/n!$ and $U^\dagger U = \mathbb{1}$. For certain times where $\omega_c t_m = 2\pi m$ (with m integer), the first exponential equals the identity, $\exp\left[-i\omega_c t a^\dagger a \right] = \exp\left[-i2\pi m a^\dagger a \right] = \mathbb{1}$, since the number operator $\hat{n} = a^\dagger a$ has an integer spectrum $0, 1, 2, \ldots$. Thus, for $t_m = (2\pi/\omega_c)m$, the full time evolution reduces to

$$e^{-iHt_m} = e^{i\frac{g^2}{\omega_c}t_m\mathcal{S}^2} = \exp\left[i2\pi m \left(g/\omega_c \right)^2 \mathcal{S}^2 \right]. \qquad (6)$$

This *exact* relation is our main result, with two major implications: (i) Our approach is not based on a perturbative argument; therefore, apart form Eq.(6), the resonator-mediated qubit-qubit interaction does not lead to any further undesired, spurious terms. (ii) Since the unitary transformation given in Eq.(6) does *not* contain any operators acting on the resonator mode, it is completely insensitive to the state of the resonator [9, 10, 12], even though the spin-spin interactions present in $\mathcal{S}^2$ have been established effectively via the resonator degrees of freedom, and thus does not require cooling the resonator mode to the ground state. For specific times, the time-evolution in the polaron and the lab-frame fully coincide and become truly independent of the phonon mode. This statement holds provided that rethermalization of the resonator mode can be neglected over the relevant gate time. The experimental implications for this condition will be discussed below.

To further illustrate Eq.(6), let us consider three paradigmatic examples [56]: (1) For longitudinal coupling ($\eta_i^z = 1$, $\eta_i^x = \eta_i^y = 0$), as could be realized (for
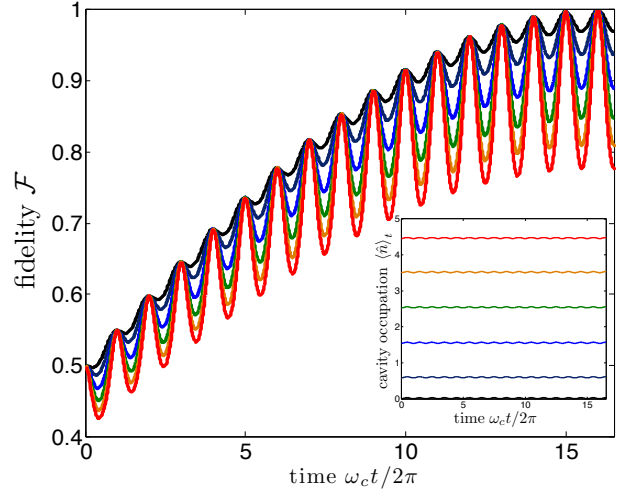

Figure 2: (color online). Fidelity $\mathcal{F}$ with the maximally entangled target state $|\Psi_{\text{tar}}\rangle = (|\Uparrow\Downarrow\rangle + i\,|\Downarrow\Uparrow\rangle)/\sqrt{2}$ for transversal coupling ($\mathcal{S} = \sigma_1^x + \sigma_2^x$), the initial product state $\rho(0) = |\Uparrow\Downarrow\rangle\langle\Uparrow\Downarrow| \otimes \rho_{\text{th}}(T)$ and different temperatures $k_B T/\omega_c = 0, 1, 2, 3, 4, 5$. Independently of the temperature T, the spins periodically disentangle from the (hot) resonator mode and systematically build-up entanglement among themselves. While the peaks are merely independent of temperature, the amplitude of the precursory oscillations do increase with temperature. Inset: Occupation of the resonator $\langle \hat{n} \rangle_t$ showing small oscillations due to weak entanglement between the qubits and the cavity mode [10]. Other numerical parameters: $\omega_q/\omega_c = \Gamma = 0$, $g/\omega_c = 1/16$, $\kappa/\omega_c = Q^{-1} = 10^{-5}$.

example) with defect spins coupled to nanomechanical oscillators [47], we can identify the effective spin-spin Hamiltonian $H_{\text{eff}} = \Omega_m (\sigma_1^z + \sigma_2^z)^2$, which results in a relative phase $\phi = 4\Omega_m$ for the states $|11\rangle = |\Uparrow\Uparrow\rangle$, $|00\rangle = |\Downarrow\Downarrow\rangle$ as compared to the states $|10\rangle$ and $|01\rangle$, respectively. By adding a local unitary on both qubits, such that $|0\rangle_i \to \exp(-i\phi/2)|0\rangle_i$ and $|1\rangle_i \to \exp(i\phi/2)|1\rangle_i$, in total for $\phi = \pi/2$ we obtain a controlled phase gate $U_{\text{Cphase}} = \text{diag}(1, 1, 1, -1)$, which gives a phase of -1 exclusively to $|11\rangle$, while leaving all other states invariant. (2) Again for longitudinal coupling ($\eta_i^z = 1$, $\eta_i^x = \eta_i^y = 0$) and $N \geq 2$ qubits, Eq.(6) results in a unitary transformation $U = \exp\left[-i\theta I_z^2\right]$ generated by a non-linear top Hamiltonian describing precession around the $I_z = \sum_i \sigma_i^z$ axis with a rate depending on the z-component of angular momentum [12]; as shown in Ref.[12], this can be used to simulate nonlinear spin models. (3) For transversal coupling with $\mathcal{S} = \sigma_1^x + \sigma_2^x$, as could be realized (for example) with quantum dot based qubits embedded in circuit-QED cavities [28, 42] or SAW cavities [43, 44], we have $\mathcal{S}^2 = 2 \times \mathbb{1} + 2\sigma_1^x\sigma_2^x$. Up to an irrelevant global phase ϕ_{gp} due to the first term $\sim \mathbb{1}$, we get

$$e^{-iHt_m} = e^{-i\phi_{\text{gp}}} \underbrace{\exp\left[i4\pi m \left(g/\omega_c \right)^2 \sigma_1^x\sigma_2^x \right]}_{\equiv U_{\text{id}}^x(m, g/\omega_c)}, \qquad (7)$$

which for $m\left(g/\omega_c\right)^2 = 1/16$ yields a maximally entangling gate, that is $U_{\mathrm{id}}^x\left(1, 1/4\right)\left|\Downarrow\Downarrow\right\rangle = \frac{1}{\sqrt{2}}\left(\left|\Downarrow\Downarrow\right\rangle + i\left|\Uparrow\Uparrow\right\rangle\right)$, $U_{\mathrm{id}}^x\left(1, 1/4\right)\left|\Uparrow\Downarrow\right\rangle = \frac{1}{\sqrt{2}}\left(\left|\Uparrow\Downarrow\right\rangle + i\left|\Downarrow\Uparrow\right\rangle\right)$ etc., i.e., initial qubit product states evolve to maximally entangled states, irrespectively of the temperature of the resonator mode, on a timescale $t_{\max} = \pi/8g_{\mathrm{eff}}$ (where $g_{\mathrm{eff}} = g^2/\omega_c$); compare Fig.2 for an exemplary time evolution, starting initially from the product state $\rho\left(0\right) = \left|\Uparrow\Downarrow\right\rangle\left\langle\Uparrow\Downarrow\right| \otimes \rho_{\mathrm{th}}\left(T\right)$, with the cavity mode in the thermal state $\rho_{\mathrm{th}}\left(T\right) = Z^{-1}\exp\left[-\beta\omega_c a^\dagger a\right]$, and $\beta = 1/k_B T$. Indeed entanglement peaks are observed at stroboscopic times ($\omega_c t_m = 2\pi m$), independent of the temperature T, eventually culminating in a maximally entangled state at time $t_{\max}$.

Coupling to environment.—In the analysis above, we have ignored the presence of decoherence, which in any realistic setting will degrade the effects of coherent qubit-resonator interactions. Therefore, we complement our analytical findings with numerical simulations of the full master equation for the system's density matrix ρ,

$$\dot{\rho} = -i\left[H, \rho\right] + \kappa\left(\bar{n}_{\mathrm{th}} + 1\right)\mathcal{D}\left[a\right]\rho + \kappa\bar{n}_{\mathrm{th}}\mathcal{D}\left[a^\dagger\right]\rho$$
$$+ \frac{\Gamma}{4}\sum_{i=1,2}\mathcal{D}\left[\sigma_i^z\right]\rho, \qquad (8)$$

where the generic spin-resonator Hamiltonian H is given in Eq.(1) and the last two dissipative terms in the first line of Eq.(8), with $\mathcal{D}\left[a\right]\rho = a\rho a^\dagger - \frac{1}{2}\left\{a^\dagger a, \rho\right\}$ and a cavity mode decay rate $\kappa = \omega_c/Q$, describe rethermalization of the cavity mode towards the thermal occupation $\bar{n}_{\mathrm{th}} = \left(\exp\left[\hbar\omega_c/k_B T\right] - 1\right)^{-1}$ at temperature T; here, Q is the quality-factor of the cavity. The last line in Eq.(8) describes dephasing of the qubits with a dephasing rate $\Gamma \sim 1/T_2^\star$, where $T_2^\star$ is the time-ensemble-averaged dephasing time. In Eq.(8) we have ignored single spin relaxation processes, since the associated timescale T_1 is typically much longer than $T_2^\star$; still, relaxation processes could be included straightforwardly in our model by adding the decay terms $\dot{\rho} = \cdots + T_1^{-1}\sum_i\mathcal{D}\left[\sigma_i^-\right]\rho$ and the corresponding error (infidelity) could be analyzed along the lines of our analysis shown below.

Numerical results.—To quantitatively capture the effects of decoherence, in the following we provide numerical results of the Master equation Eq.(8), for the initial product state $\rho\left(0\right) = \left|\Uparrow\Downarrow\right\rangle\left\langle\Uparrow\Downarrow\right| \otimes \rho_{\mathrm{th}}\left(T\right)$, with the cavity mode in the thermal state $\rho_{\mathrm{th}}\left(T\right) = Z^{-1}\exp\left[-\beta\omega_c a^\dagger a\right]$, and (transversal) spin-resonator coupling with $\eta_i^x = 1$ and $\eta_i^y = \eta_i^z = 0$. As a figure of merit for our protocol, we consider the logarithmic negativity $E_\mathcal{N}$ (which ranges between 0 for separable states to at maximum 1 for two maximally-entangled qubits) to quantify the entanglement between the two qubits, and the state fidelity $\mathcal{F} = \left\langle\Psi_{\mathrm{tar}}|\varrho|\Psi_{\mathrm{tar}}\right\rangle$ with the maximally entangled target state $\left|\Psi_{\mathrm{tar}}\right\rangle = \left(\left|\Uparrow\Downarrow\right\rangle + i\left|\Downarrow\Uparrow\right\rangle\right)/\sqrt{2}$; here, with $\mathrm{tr}_a\left[\ldots\right]$ denoting the trace over the resonator degrees of freedom, $\varrho = \mathrm{tr}_a\left[\rho\right]$ refers to the density matrix of the qubits. As

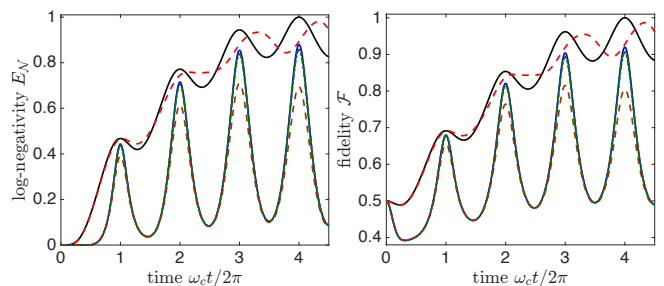Figure 3: (color online). Logarithmic negativity $E_\mathcal{N}$ (left) and fidelity $\mathcal{F}$ (right) in the presence of noise. As a benchmark, the solid (topmost) black line refers to the quasi-ideal limit ($\Gamma = 0$, $\kappa/\omega_c = Q^{-1} = 10^{-5}$ and $k_B T/\omega_c = 0$), while the red dashed curve accounts for a non-zero qubit level splitting $\omega_q/\omega_c = 0.1$. The solid blue line also accounts for dephasing of the qubits with a (rather large) dephasing rate $\Gamma/\omega_c = 1\%$ and finite thermal occupation of the resonator mode with $k_B T/\omega_c = 5$ ($\bar{n}_{\mathrm{th}} \approx 4.5$). The results are relatively insensitive to the quality factor of the cavity, provided that $\kappa_{\mathrm{eff}} \ll \Gamma$; the green dash-dotted line (where $Q = 10^3$) is basically identical to the $Q = 10^5$ scenario, whereas the brown dashed (lowest) one with $Q = 10^2$ (that is, $\kappa/\omega_c = \Gamma/\omega_c = 1\%$) shows a clear reduction in $E_\mathcal{N}$ and $\mathcal{F}$. This result can be traced back to the hot-gate requirement given in Eq.(9). Ideally, maximum entanglement is reached for $f_c t = 4$, with several precursory oscillation peaks at $f_c t = 1, 2, 3$. Other numerical parameters: $g/\omega_c = 1/8$, $\omega_q/\omega_c = 0$ (except for the red dashed curve where $\omega_q/\omega_c = 0.1$).

shown in Ref.[51], similar results can be obtained for the average gate fidelity. Typical results from our numerical simulations in the presence of noise are displayed in Fig.3. As expected from our analytical results, for $\omega_c t_m = 2\pi m$ the two qubits disentangle from the thermally populated resonator mode and systematically evolve towards the maximally entangled target state $\left|\Psi_{\mathrm{tar}}\right\rangle$; for example, for $g/\omega_c = 1/8$ (as used in Fig.3), the spins evolve towards $U_{\mathrm{id}}^x\left(1, 1/8\right)\left|\Uparrow\Downarrow\right\rangle = \cos\left(\pi/16\right)\left|\Uparrow\Downarrow\right\rangle + i\sin\left(\pi/16\right)\left|\Downarrow\Uparrow\right\rangle$ for $m = 1$, $U_{\mathrm{id}}^x\left(2, 1/8\right)\left|\Uparrow\Downarrow\right\rangle = \cos\left(\pi/8\right)\left|\Uparrow\Downarrow\right\rangle + i\sin\left(\pi/8\right)\left|\Downarrow\Uparrow\right\rangle$ for $m = 2$, and $U_{\mathrm{id}}^x\left(3, 1/8\right)\left|\Uparrow\Downarrow\right\rangle = \cos\left(3\pi/16\right)\left|\Uparrow\Downarrow\right\rangle + i\sin\left(3\pi/16\right)\left|\Downarrow\Uparrow\right\rangle$ for $m = 3$, before the entanglement build-up culminates in the fully-entangling dynamics $U_{\mathrm{id}}^x\left(4, 1/8\right)\left|\Uparrow\Downarrow\right\rangle = \left(\left|\Uparrow\Downarrow\right\rangle + i\left|\Downarrow\Uparrow\right\rangle\right)/\sqrt{2}$. For all practical purposes, this statement holds independently of the temperature T and the associated thermal occupation of the resonator mode $\bar{n}_{\mathrm{th}} \approx k_B T/\hbar\omega_c$, provided that the quality factor of the cavity Q is sufficiently high; a quantitative statement specifying this regime will be given below. Moreover, while our analytical treatment has assumed $\omega_q = 0$, we have numerically verified that the proposed protocol is robust against non-zero level splittings of the qubits $\omega_q/\omega_c \lesssim 0.1$; compare the dashed line in Fig.3 and further information provided in Ref.[51].

Gate time requirements: Error scaling.—As described by Eq.(8), coupling to the environment leads to two dominant error sources: (i) rethermalization of the resonator
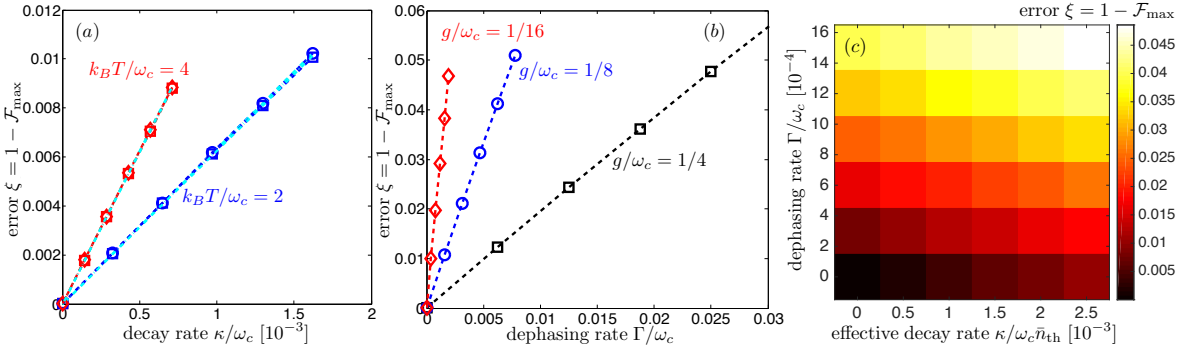
Figure 4: (color online). Errors ($\xi = 1 - \mathcal{F}_{\max}$) due to rethermalization of the cavity mode (a) and qubit dephasing (b). (a) Rethermalization-induced error for $k_B T/\omega_c = 2$ (blue) and $k_B T/\omega_c = 4$ (red), and $\Gamma = 0$. The error ξ_κ is found to be independent of $\mu = g/\omega_c$: $\mu = 1/16$ (squares) and $\mu = 1/8$ (blue circles and red diamonds). (b) Dephasing induced errors for $\mu = 1/4$ (squares), $\mu = 1/8$ (circles) and $\mu = 1/16$ (diamonds); here, $\kappa/\omega_c = 10^{-6}$ and $k_B T/\omega_c = 0.01$. In both cases the linear error scaling is verified. Other numerical parameters: $\omega_q/\omega_c = 0$. (c) Total error ξ as a function of both the effective rethermalization rate $\sim \kappa/\omega_c \bar{n}_{\mathrm{th}} \sim \bar{n}_{\mathrm{th}}/Q$ and the spin dephasing rate $\sim \Gamma/\omega_c$ for $g/\omega_c = 1/16$, $k_B T/\omega_c = 2$ and $\omega_q = 0$.

mode with an effective rate $\sim \kappa \bar{n}_{\mathrm{th}}$, and (ii) dephasing of the qubits on a timescale $\sim T_2^\star$. For any *hot* gate, the associated gate time $t_{\mathrm{gate}} \sim g_{\mathrm{eff}}^{-1}$, with $g_{\mathrm{eff}} = g^2/\omega_c = \mu^2 \omega_c$, has to be shorter than the time-scale associated with the effective (thermally-enhanced) rethermalization rate $\kappa_{\mathrm{eff}} = \kappa \bar{n}_{\mathrm{th}} \approx k_B T/Q$; the last approximation holds for $k_B T \gg \omega_c$. For the gate described above [see Eq.(6)], this directly leads to the requirement

$$g^2/\omega_c \gg k_B T/Q \quad \Leftrightarrow \quad k_B T \ll Q\mu^2 \omega_c. \qquad (9)$$

Thus, for $T = 1$K ($k_B T/2\pi \approx 20$GHz) and a cavity quality factor $Q \approx 10^5 - 10^6$, we need $g_{\mathrm{eff}}/2\pi \gg (20 - 200)$ kHz. Provided that our assumption $\omega_c \gg \omega_q$ is still fulfilled, for fixed temperature T, quality factor Q and coupling g, relation (9) may be conveniently fulfilled by choosing ω_c sufficiently small, up to the lower limit $\omega_c \geq 4g$ (which is needed to fulfill $m \geq 1$ [51]) and at the cost of a potentially relatively large device (since the device dimensions scale with $\sim \lambda_c \sim \omega_c^{-1}$). Conversely, for fixed $\mu = g/\omega_c$ [26, 44, 52], Eq.(9) can be achieved by choosing ω_c sufficiently large. In addition, the gate time has to be short compared to the qubit's dephasing time $T_2^\star \sim \Gamma^{-1}$, which gives the second requirement

$$g^2/\omega_c \gg \Gamma \quad \Leftrightarrow \quad \Gamma \ll \mu^2 \omega_c. \qquad (10)$$

For concreteness, let us consider a specific setup where conditions (9) and (10) can be met with state-of-the-art technology: Quantum dots (QDs) have been successfully integrated with superconducting microwave cavities, with a relatively large charge-cavity coupling of $g_{\mathrm{ch}}/2\pi \sim (20 - 100)$ MHz [34–37, 39]. For QD spin qubits a vacuum Rabi frequency of $g_{\mathrm{sp}}/2\pi \sim 1$MHz has been predicted [27, 28, 35], with the potential to increase this coupling to ~ 10MHz with new, recently demonstrated cavity designs [53]. Furthermore, for superconducting transmission line resonators quality fac-

tors $Q \sim 10^6$ have been demonstrated [54]. Then, taking $g_{\mathrm{sp}}/2\pi = 10$MHz, $\omega_c/2\pi \approx (0.16 - 1)$GHz, i.e., $g_{\mathrm{eff}}/2\pi \approx (0.1 - 0.6)$MHz, and $Q = 10^6$, conditions (9) and (10) can be met simultaneously for temperatures $T \sim 1$K [since $T \ll 5(30)$K to fulfill condition (9) for $g_{\mathrm{eff}}/2\pi \approx 0.1(0.6)$MHz] and dephasing timescales $T_2^\star \sim 100\mu$s [since $\Gamma/2\pi \ll (0.1 - 0.6)$ MHz to fulfill condition (10)], as has been demonstrated with isotopically purified Si samples [55]. Therefore, a faithful implementation of our gate will *not* require cooling to milli-Kelvin temperatures. Similar promising estimates also apply to spin-qubits coupled to SAW-resonators [51].

In the following, we quantify the infidelities induced by the two error sources outlined above: Rethermalization of the resonator mode during the gate leads to errors (infidelities) if the resonator is entangled with the qubits. Due to leakage of which-way information, resonator noise leads to qubit dephasing at a rate proportional to the relevant separation in phase space, that is the square of the resonator displacement $\mu = g/\omega_c$ [47]. The effective rethermalization-induced dephasing rate for the qubits is then $\Gamma_{\mathrm{eff}} \sim \kappa \bar{n}_{\mathrm{th}} (g/\omega_c)^2$. To obtain a simple estimate for the rethermalization-induced error, this effective rate Γ_{eff} is multiplied with the relevant gate time which scales as $t_{\mathrm{gate}} \sim \omega_c/g^2$, yielding the error $\xi_\kappa \sim (\kappa/\omega_c) \bar{n}_{\mathrm{th}}$, which is *independent* of the spin-resonator coupling strength g [24, 47, 51]. However, since the overall gate time $t_{\mathrm{gate}} \sim \omega_c/g^2$ increases for small $\mu = g/\omega_c$, errors will accumulate due to direct qubit decoherence processes. Accordingly, errors due to qubit dephasing are expected to scale as $\xi_\Gamma \sim \Gamma/g_{\mathrm{eff}} \sim \mu^{-2}\Gamma/\omega_c$. This simple linear scaling holds for a Markovian noise model where qubit dephasing is described by a standard pure dephasing term [compare Eq.(8)] leading to an exponential loss of coherence $\sim \exp[-t/T_2^\star]$; note that for non-Markovian qubit dephasing a better, sub-linear scaling can be expected [43, 47]. For small infidelities ($g_{\mathrm{eff}} \gg \kappa_{\mathrm{eff}}, \Gamma$), the indi-

vidual linear error terms due to cavity rethermalization and qubit dephasing can be added independently, yielding the total error

$$\xi \approx \alpha_\kappa \left(\kappa/\omega_c\right) \bar{n}_{\mathrm{th}} + \alpha_\Gamma \Gamma/\omega_c. \tag{11}$$

This simple linear error model has been verified numerically; compare Fig.4. Based on these results we extract the coefficients $\alpha_\kappa \approx 4$ (which is approximately independent of g [24, 51]) and $\alpha_\Gamma \approx 0.1/\mu^2$, i.e., $\alpha_\Gamma \approx 26(6.5)$ for $\mu = 1/16(1/8)$. For $g_{\mathrm{sp}}/2\pi \approx 10\mathrm{MHz}$ [27, 28, 53], a relatively low resonator frequency $\omega_c/2\pi = 16g_{\mathrm{sp}}/2\pi = 160\mathrm{MHz}$, $T = 1\mathrm{K}$ (corresponding to $\bar{n}_{\mathrm{th}} \approx 130$), $Q = 10^5$ [53, 54] and a realistic dephasing rate $\Gamma/2\pi \approx 0.1\mathrm{MHz}$ [55], that is $\kappa/\omega_c\bar{n}_{\mathrm{th}} \approx 1.3 \times 10^{-3}$ and $\Gamma/\omega_c \approx 6 \times 10^{-4}$, our estimates then predict an overall infidelity of $\xi \approx 2\%$, with the potential to reach error rates $\xi \approx 0.2\%$ below the threshold for quantum error correction for state-of-the-art experimental parameters ($Q \approx 10^6$, $\Gamma/2\pi \approx 10\mathrm{kHz}$) [4, 54, 55]. This simple estimate is corroborated by numerical simulations that fully account for higher-order errors; compare the density plot in Fig.4(c). Note that the error estimate given in Eq.(11) assumes perfect timing of the gate, as the maximum fidelity is reached exactly at time t_{max}, whereas under experimentally realistic conditions there will be a residual error due to imperfect timing of the gate. However, as shown in Ref.[51], for sufficiently small, but realistic timing accuracies of $(\omega_c/2\pi)\,\Delta t \lesssim 1\%$ and small spin-resonator coupling $g/\omega_c \lesssim 1/16$ (implying small oscillation amplitudes), the effects of time-jitter become negligible.

Conclusions & Outlook.—To conclude, we have proposed and analyzed a high-fidelity hot gate for generic spin-resonator systems which allows for coherent spin-spin coupling, even in the presence of a thermally populated resonator mode. While we have mostly focused on just two spins, our scheme fully applies to more than two spins, which should allow for the preparation of maximally entangled multi-partite states; as shown in Ref.[11] in the context of trapped ions, a propagator of the form given in Eq.(6) applied to the initial product state $|00\cdots0\rangle$ may be used to generate states of the form $1/\sqrt{2}\left(|00\cdots0\rangle + e^{i\phi}|11\cdots1\rangle\right)$, where $|00\cdots0\rangle$ and $|11\cdots1\rangle$ are product states with all qubits in the same state $|0\rangle$ or $|1\rangle$, respectively.

[1] R. Hanson and D. D. Awschalom, Nature **453**, 1043 (2008).
[2] M. A. Nielsen and I. L. Chuang, Quantum Computation and Quantum Information (Cambridge University Press, 2010).
[3] L. R. Schreiber and H. Bluhm, Nature Nanotech. **9**, 966 (2014).
[4] E. Knill, Nature **434**, 39 (2005).
[5] N. H. Nickerson, Y. Li, and S. C. Benjamin, Nat. Commun. **4**, 1756 (2013).
[6] J. Majer *et al.*, Nature **449**, 443 (2007).
[7] M. A. Sillanpää, J. I. Park, and R. W. Simmonds, Nature **449**, 438 (2007).
[8] F. Schmidt-Kaler *et al.*, Nature **422**, 408 (2003).
[9] A. Soerensen and K. Moelmer, Phys. Rev. Lett. **82**, 1971 (1999).
[10] A. Soerensen and K. Moelmer, Phys. Rev. A **62**, 022311 (2000).
[11] K. Moelmer and A. Soerensen, Phys. Rev. Lett. **82**, 1835 (1999).
[12] G. J. Milburn, arXiv:quant-ph/9908037 (unpublished).
[13] G. J. Milburn, S. Schneider, and D. F. V. James, Fortschr. Phys. **48**, 801 (2000).
[14] J. F. Poyatos, J. I. Cirac, and P. Zoller, Phys. Rev. Lett. **81**, 1322 (1998).
[15] J. I. Cirac and P. Zoller, Nature **404**, 579 (2000).
[16] J. J. Garcia-Ripoll, P. Zoller, and J. I. Cirac, Phys. Rev. Lett. **91**, 157901 (2003).
[17] J. J. Garcia-Ripoll, P. Zoller, and J. I. Cirac, Phys. Rev. A **71**, 062309 (2005).
[18] D. Porras and J. I. Cirac, Phys. Rev. Lett. **92**, 207901 (2004).
[19] D. Leibfried *et al.*, Nature **422**, 412 (2003).
[20] G. Kirchmair, J. Benhelm, F. Zähringer, R. Gerritsma, C. F. Roos and R. Blatt, New J. Phys. **11**, 023002 (2009).
[21] D. J. Reilly, NPJ Quantum Information **1**, 15011 (2015).
[22] P. Treutlein, C. Genes, K. Hammerer, M. Poggio, and P. Rabl, "Hybrid Mechanical Systems", in: "Cavity Optomechanics", ed. by M. Aspelmeyer, T. J. Kippenberg, and F. Marquardt (Springer, Berlin 2014) pp. 327-351.
[23] A. Blais, R.-S. Huang, A. Wallraff, S. M. Girvin, and R. J. Schoelkopf, Phys. Rev. A **69**, 062320 (2004).
[24] B. Royer, A. L. Grimsmo, N. Didier, and A. Blais, arXiv:1603.04424 (unpublished).
[25] L. Childress, A. S. Soerensen, and M. D. Lukin, Phys. Rev. A **69**, 042302 (2004).
[26] J. M. Taylor and M. D. Lukin, arXiv:cond-mat/0605144 (unpublished).
[27] P.-Q. Jin, M. Marthaler, A. Shnirman, and G. Schön, Phys. Rev. Lett. **108**, 190506 (2012).
[28] X. Hu, Y.-x. Liu, and F. Nori, Phys. Rev. B **86**, 035314 (2012).
[29] M. Trif, V. N. Golovach, and D. Loss, Phys. Rev. B **77**, 045434 (2008).
[30] M. J. Gullans, Y.-Y. Liu, J. Stehlik, J. R. Petta, and J. M. Taylor, Phys. Rev. Lett. **114**, 196802 (2015).
[31] P.-Q. Jin, M. Marthaler, J. H. Cole, A. Shnirman, and G. Schön, Phys. Rev. B **84**, 035322 (2011).
[32] M. Kulkarni, O. Cotlet, and H. E. Türeci, Phys. Rev. B **90**, 125402 (2014).
[33] V. Srinivasa, J. M. Taylor, and C. Tahan,

arXiv:1603.04829 (unpublished).

[34] T. Frey, P. J. Leek, M. Beck, A. Blais, T. Ihn, K. Ensslin, and A. Wallraff, Phys. Rev. Lett. **108**, 046807 (2012).

[35] K. D. Petersson, L. W. McFaul, M. D. Schroer, M. Jung, J. M. Taylor, A. A. Houck, and J. R. Petta, Nature **490**, 380 (2012).

[36] Y.-Y. Liu, K. D. Petersson, J. Stehlik, J. M. Taylor, and J. R. Petta, Phys. Rev. Lett. **113**, 036801 (2014).

[37] H. Toida, N. Nakajima, and S. Komiyama, Phys. Rev. Lett. **110**, 066802 (2013). Also see: A. Wallraff, A. Stockklauser, T. Ihn, J. R. Petta, and A. Blais, Phys. Rev. Lett. **111**, 249701 (2013).

[38] M. R. Delbecq, V. Schmitt, F. D. Parmentier, N. Roch, J. J. Viennot, G. Feve, B. Huard, C. Mora, A. Cottet, and T. Kontos, Phys. Rev. Lett. **107**, 256804 (2011).

[39] J. J. Viennot, M. R. Delbecq, M. C. Dartiailh, A. Cottet, and T. Kontos, Phys. Rev. B **89**, 165404 (2014).

[40] J. J. Viennot, M. C. Dartiailh, A. Cottet, and T. Kontos, Science **349**, 408 (2015).

[41] L. J. Zou, D. Marcos, S. Diehl, S. Putz, J. Schmiedmayer, J. Majer, and P. Rabl, Phys. Rev. Lett. **113**, 023603 (2014).

[42] F. Beaudoin, D. Lachance-Quirion, W. A. Coish, M. Pioro-Ladriere, arXiv:1606.04736 (unpublished).

[43] M. J. A. Schuetz, E. M. Kessler, G. Giedke, L. M. K. Vandersypen, M. D. Lukin, and J. I. Cirac, Phys. Rev. X **5**, 031031 (2015).

[44] J. C. Chen, Y. Sato, R. Kosaka, M. Hashisaka, K. Muraki, and T. Fujisawa, Sci. Rep. **5**, 15176 (2015).

[45] D. A. Golter, T. Oo, M. Amezcua, K. A. Stewart, and H. Wang, Phys. Rev. Lett. **116**, 143602 (2016).

[46] P. Rabl, P. Cappellaro, M. V. Gurudev Dutt, L. Jiang, J. R. Maze, and M. D. Lukin, Phys. Rev. B **79**, 041302(R) (2009).

[47] P. Rabl, S. J. Kolkowitz, F. H. L. Koppens, J. G. E. Harris, P. Zoller, and M. D. Lukin, Nat. Phys. **6**, 602 (2010).

[48] K. V. Kepesidis, S. D. Bennett, S. Portolan, M. D. Lukin, and P. Rabl, Phys. Rev. B **88**, 064105 (2013).

[49] S. D. Bennett, N. Y. Yao, J. Otterbach, P. Zoller, P. Rabl, and M. D. Lukin, Phys. Rev. Lett. **110**, 156402 (2013).

[50] A. Palyi, P. R. Struck, M. Rudner, K. Flensberg, and G. Burkard, Phys. Rev. Lett. **108**, 206811 (2012).

[51] See Supplemental Material for details.

[52] R. J. Schoelkopf and S. M. Girvin, Nature **451**, 664 (2008).

[53] N. Samkharadze, A. Bruno, P. Scarlino, G. Zheng, D. P. DiVincenzo, L. DiCarlo, and L. M. K. Vandersypen, Phys. Rev. Applied **5**, 044004 (2016).

[54] R. Barends, J. J. A. Baselmans, S. J. C. Yates, J. R. Gao, J. N. Hovenier, and T. M. Klapwijk, Phys. Rev. Lett. **100**, 257002 (2008).

[55] M. Veldhorst *et al.*, Nature Nano. **9**, 981 (2014).

[56] Strictly speaking, for $\omega_q = 0$ the three examples considered differ by a global unitary only. However, even if this symmetry is broken by small, but finite qubit level splittings $\omega_q > 0$, our findings (approximately) still prevail.

Supplemental Material for:
High-Fidelity Hot Gates for Generic Spin-Resonator Systems

M. J. A. Schuetz,[1] G. Giedke,[2,3] L. M. K. Vandersypen,[4] and J. I. Cirac[1]

[1]*Max-Planck-Institut für Quantenoptik, Hans-Kopfermann-Str. 1, 85748 Garching, Germany*
[2]*Donostia International Physics Center, Paseo Manuel de Lardizabal 4, 20018 Donostia-San Sebastián, Spain*
[3]*Ikerbasque, Basque Foundation for Science, Maria Diaz de Haro 3, 48013 Bilbao, Spain*
[4]*Kavli Institute of NanoScience, TU Delft, P.O. Box 5046, 2600 GA Delft, The Netherlands*

I. THERMAL OCCUPATION

Here, we first provide typical thermal occupation numbers $\bar{n}_{\text{th}}$ for relevant experimental parameter regimes. At a temperature $T = 4\text{K}$, a (mechanical) oscillator of frequency $\omega_c/2\pi \sim (1-10)\,\text{GHz}$ has an thermal equilibrium occupation number much larger than one, $\bar{n}_{\text{th}} \approx 8 - 80$: compare Fig.S1.

II. POLARON VS. LAB FRAME

In this Appendix we show that for stroboscopic times the ideal time evolution in the lab frame fully coincides with the one in the polaron frame.

In the ideal (noise-free) scenario, the evolution of the system in the lab frame, comprising both spin and resonator degrees of freedom, is described by Schrödinger's equation

$$i\frac{d}{dt}\left|\psi\right\rangle_t = H\left|\psi\right\rangle_t. \tag{S1}$$

In the polaron frame, the time evolution is governed by

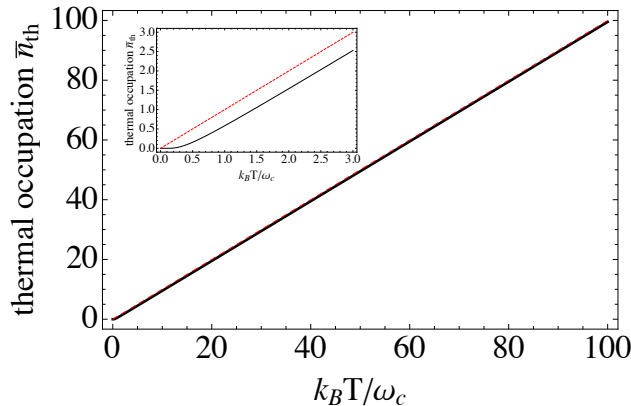$$i\frac{d}{dt}|\tilde{\psi}\rangle_t = H_0|\tilde{\psi}\rangle_t, \tag{S2}$$

Figure S1: (color online). Thermal occupation $\bar{n}_{\text{th}} = (\exp[\hbar\omega_c/k_B T] - 1)^{-1}$ (black solid line) and high-temperature approximate result $\bar{n}_{\text{th}} \approx k_B T/\hbar\omega_c$ (red dashed line). For $T = 4\text{K}$ and $\omega_c/2\pi = 1\text{GHz}$ ($\omega_c/2\pi = 10\text{GHz}$), we have $k_B T/\hbar\omega_c \approx 80$ ($k_B T/\hbar\omega_c \approx 8$). For $T = 1\text{K}$ and $\omega_c/2\pi = 1\text{GHz}$ ($\omega_c/2\pi = 10\text{GHz}$), we have $\bar{n}_{\text{th}} \approx 20$ ($\bar{n}_{\text{th}} \approx 2$).

where $|\tilde{\psi}\rangle_t = U^\dagger\left|\psi\right\rangle_t$, $U = \exp\left[\mu S\left(a - a^\dagger\right)\right]$, and $H_0 = U^\dagger H U = \omega_c a^\dagger a - \frac{g^2}{\omega_c}\mathcal{S}^2$; the polaron transformation U entangles spin with resonator degrees of freedom. The solution to Eq.(S2) reads $|\tilde{\psi}\rangle_t = \exp[-iH_0 t]\,|\tilde{\psi}\rangle_0$. Using the relation $\exp\left[-i\omega_c t a^\dagger a\right] = \exp\left[-i2\pi m a^\dagger a\right] = \mathbb{1}$ for stroboscopic times ($\omega_c t_m = 2\pi m$, with m integer), full time evolution in the polaron frame reduces to

$$|\tilde{\psi}\rangle_{t_m} = e^{i2\pi m\mu^2\mathcal{S}^2}|\tilde{\psi}\rangle_0. \tag{S3}$$

Transforming back to the lab frame with $|\tilde{\psi}\rangle_t = U^\dagger\left|\psi\right\rangle_t$, and using that U commutes with the propagator $\exp\left[i2\pi m\mu^2\mathcal{S}^2\right]$, we obtain the (stroboscopic) solution in the lab frame, $\left|\psi\right\rangle_{t_m} = e^{i2\pi m\mu^2\mathcal{S}^2}\left|\psi\right\rangle_0$, which fully coincides with the one in the polaron frame.

III. GATE TIME

Ideally, the gate time t_{gate} has to fulfill two conditions: (i) it has to be chosen stroboscopically, that is $\omega_c t_{\text{gate}} = 2\pi m$, with $m = 1, 2, \ldots$ with (ii) the parameters such that $m\mu^2 = 1/16$ in order to obtain a maximally-entangling gate (in the absence of noise). Combination of (i) and (ii) then yields the ideal gate time

$$t_{\text{max}} = \frac{\pi}{8g_{\text{eff}}}, \tag{S4}$$

as given in the main text. The gate time t_{max} should be short compared to the relevant noise timescales, which yields the requirement $g_{\text{eff}} \gg \kappa_{\text{eff}}, \Gamma$. In principle, large values of $g_{\text{eff}} = g^2/\omega_c$ can be obtained by choosing the resonator frequency ω_c sufficiently small, provided that ω_c can be tuned independently of g. This can be done up to the lower bound $\omega_c \geq 4g$ which follows directly from the requirement $m = 1/(16\mu^2) \geq 1$.

IV. SPIN-SPIN COUPLING IN DISPERSIVE REGIME

We consider two identical spins homogeneously coupled to a common resonator mode. The dynamics are assumed to be governed by the Jaynes-Cummings Hamil-

tonian

$$H = \Delta\left(S_1^z + S_2^z\right) + g\left[a\left(S_1^+ + S_2^+\right) + a^\dagger\left(S_1^- + S_2^-\right)\right], \tag{S5}$$

which is valid within the rotating-wave approximation for $\sqrt{\bar{n}_{\rm th}}g, \Delta \ll \omega_c$, with the detuning $\Delta = \omega_q - \omega_c$. In the following we consider the *dispersive regime*, where the spin-resonator coupling is strongly detuned ($\sqrt{\bar{n}_{\rm th}}g \ll \Delta$). In this regime, the spin-resonator coupling can be treated perturbatively. To stress the perturbative treatment we write

$$\begin{align} H &= H_0 + H_1, \tag{S6}\\ H_0 &= \Delta S^z, \tag{S7}\\ H_1 &= g\left(aS^+ + a^\dagger S^-\right), \tag{S8} \end{align}$$

where $S^\alpha = S_1^\alpha + S_2^\alpha$ (for $\alpha = \pm, z$) are collective spin operators. We perform a standard Schrieffer-Wolff transformation

$$\begin{align} \tilde{H} &= e^A H e^{-A} \tag{S9}\\ &\approx H_0 + H_1 + [A, H_0 + H_1] + \frac{1}{2}[A, [A, H_0]] \tag{S10} \end{align}$$

where the operator A (with $A^\dagger = -A$) is assumed to have a perturbative expansion in g, i.e., $A = 0 + \mathcal{O}(g) + \dots$ By choosing

$$[A, H_0] = -H_1, \tag{S11}$$

one obtains a Hamiltonian $\tilde{H}$ without linear coupling in g,

$$\tilde{H} \approx H_0 + \frac{1}{2}[A, H_1]. \tag{S12}$$

For the Hamiltonian given in Eq.(S6), the condition in Eq.(S11) is fulfilled by the choice

$$A = \frac{g}{\Delta}\left(aS^+ - a^\dagger S^-\right), \tag{S13}$$

which yields the Hamiltonian

$$\tilde{H} \approx \left(\Delta + \frac{g^2}{\Delta} + 2\frac{g^2}{\Delta}a^\dagger a\right)S^z + \frac{g^2}{\Delta}\left(S_1^+ S_2^- + S_1^- S_2^+\right). \tag{S14}$$

Here, the last two terms describe a cavity-state dependent dispersive shift of the qubit transition frequencies and spin-spin coupling via virtual occupation of the cavity mode, respectively. The strength of the effective spin-spin coupling is given by

$$g_{\rm eff} = \frac{g^2}{\Delta} = \frac{\epsilon}{\sqrt{\bar{n}_{\rm th}}}g, \tag{S15}$$

where we have set $\sqrt{\bar{n}_{\rm th}}g/\Delta = \epsilon \ll 1$ in order to reach the regime of validity for Eq.(S14), given by

$$\sqrt{\bar{n}_{\rm th}}g \ll \Delta \ll \omega_c. \tag{S16}$$

By transforming the Hamiltonian given in Eq.(S14) back into the lab-frame, we recover the result presented in Ref.[S1], namely

$$\begin{align} H &\approx \left[\omega_c + 2\frac{g^2}{\Delta}\left(S_1^z + S_2^z\right)\right]a^\dagger a + \left(\omega_q + \frac{g^2}{\Delta}\right)\left(S_1^z + S_2^z\right)\\ &\quad + \frac{g^2}{\Delta}\left(S_1^+ S_2^- + S_1^- S_2^+\right). \tag{S17} \end{align}$$

Here, spins and cavity mode are still coupled by the ac Stark shift term $\sim a^\dagger a$. Accordingly, one obtains an effective pure spin Hamiltonian with flip-flop interactions provided that one can neglect any fluctuations of the photon number $a^\dagger a \to \bar{n} = \langle a^\dagger a\rangle$, where $\bar{n}$ is the average number of photons in the cavity mode [S2].

Since the operator $S^z a^\dagger a$ in Eq.(S14) has an integer spectrum, one may wonder whether for stroboscopic times the spins disentangle from the resonator mode here as well. Thus, let us consider the full time evolution generated by Eq.(S5)

$$\begin{align} e^{-iHt} &= e^{-iU^\dagger \tilde{H}Ut} = U^\dagger e^{-i\tilde{H}t}U \tag{S18}\\ &\approx U^\dagger\left[\exp\left[-it\left(\delta + \tilde{\delta}a^\dagger a\right)S^z\right.\right.\\ &\quad \left.\left. -i\tilde{g}t\left(S_1^+ S_2^- + S_1^- S_2^+\right)\right]\right]U, \tag{S19} \end{align}$$

with $U = \exp(A)$, $\delta = \Delta + g^2/\Delta$, $\tilde{\delta} = 2g^2/\Delta$ and $\tilde{g} = g^2/\Delta$. Note that Eq.(S19) is an approximate statement, relying on a perturbative expansion in the coupling g. Since the flip-flop interaction conserves S^z, we find

$$e^{-iHt} \approx U^\dagger e^{-i\delta t S^z} e^{-i\tilde{\delta}t S^z a^\dagger a} e^{-i\tilde{g}t\left(S_1^+ S_2^- + S_1^- S_2^+\right)}U. \tag{S20}$$

For stroboscopic times $\tilde{\delta}t = 2\pi m$, $e^{-i\tilde{\delta}t S^z a^\dagger a} = \mathbb{1}$, yielding

$$e^{-iHt} \approx U^\dagger e^{-iH_{\rm spin}t}U, \tag{S21}$$

where $H_{\rm spin} = \delta S^z + \tilde{g}\left(S_1^+ S_2^- + S_1^- S_2^+\right)$ is a pure spin Hamiltonian, without any coupling to the resonator mode. However, in contrast to our scheme presented in the main text, the full time evolution does not reduce to a pure spin problem, since the Schrieffer-Wolff transformation $U = \exp\left[\frac{g}{\Delta}\left(aS^- - a^\dagger S^+\right)\right]$ does not commute with $e^{-iH_{\rm spin}t}$, but rather entangles the qubits with the resonator mode.

V. SCHRIEFFER-WOLFF TRANSFORMATION

If one restricts oneself to the regime $g \ll \omega_c$, the result stated in Eqn.(6) may also be derived in the perturbative framework of a Schrieffer-Wolff transformation. For concreteness, assuming $\omega_q = 0$, we consider the Hamiltonian

$$H = \underbrace{\omega_c a^\dagger a}_{H_0} + \underbrace{gS^x \otimes \left(a + a^\dagger\right)}_{V}, \tag{S22}$$

where $S^x = \sum_i \eta_i^x \sigma_i^x$ is a collective operator. In the following, and contrary to our general analysis in the main text, we restrict ourselves to the regime where the spin-resonator coupling V can be treated perturbatively with respect to H_0, that is $g \ll \omega_c$. Performing a Schrieffer-Wolff transformation $\tilde{H} = e^A H e^{-A}$ as presented in Sec. IV, with $A = -\frac{g}{\omega_c} S^x (a - a^\dagger)$, we obtain an effective Hamiltonian $\tilde{H}$ where the slow subspace is decoupled from the fast subspace up to second order in g. Explicitly it reads [compare Eq.(6)]

$$\tilde{H} \approx \omega_c a^\dagger a - \frac{g^2}{\omega_c} S_x^2. \tag{S23}$$

VI. NON-ZERO QUBIT LEVEL SPLITTING

In our derivation of Eq.(7), starting from the generic spin-resonator Hamiltonian given in Eq.(1), we have assumed $\omega_q = 0$. As demonstrated also numerically in Section VIII below, small level splittings with $\omega_q \approx 0.1\omega_c$ may still be tolerated without a significant loss in the amount of generated entanglement and the fidelity with the maximally entangled target state.

In this Appendix we investigate analytically the effects associated with a finite splitting $\omega_q > 0$. In this case, Eq.(4) can be generalized straightforwardly to

$$H = U[\underbrace{\omega_c a^\dagger a - \frac{g^2}{\omega_c} \mathcal{S}^2}_{H_0} + \frac{\omega_q}{2} \tilde{S}^z] U^\dagger, \tag{S24}$$

where $\tilde{S}^z = U^\dagger S^z U$, with $U = \exp\left[\frac{g}{\omega_c} \mathcal{S} (a - a^\dagger)\right]$. In what follows, we restrict ourselves to the (experimentally) most relevant regime where $\mu = g/\omega_c \ll 1$, which allows for a simple perturbative treatment. Expansion in the small parameter μ yields

$$\tilde{S}^z \approx S^z - \mu (a - a^\dagger)[\mathcal{S}, S^z] + \frac{\mu^2}{2} (a - a^\dagger)^2 [\mathcal{S}, [\mathcal{S}, S^z]]. \tag{S25}$$

Specifically, for $\mathcal{S} = \sum_i \sigma_i^x$ (as considered in the main text) we then obtain

$$\tilde{S}^z \approx S^z + 2i\frac{g}{\omega_c} S^y (a - a^\dagger) + 2\left(\frac{g}{\omega_c}\right)^2 S^z (a - a^\dagger)^2, \tag{S26}$$

which leads to an additional (undesired) contribution in Eq.(S24) of the form

$$\frac{\omega_q}{2} \tilde{S}^z \approx \frac{\omega_q}{2} S^z + \epsilon \left[ig S^y (a - a^\dagger) + \frac{g^2}{\omega_c} S^z (a - a^\dagger)^2 \right]. \tag{S27}$$

Here, in contrast to the ideal Hamiltonian H_0 in Eq.(S24) the spins are not decoupled from the (hot) resonator mode. However, apart from being detuned by at least

$\omega_c - \omega_q$, the undesired terms—that lead to entanglement of the spins with the (hot) resonator mode—are suppressed by the small parameter $\epsilon = \omega_q/\omega_c \ll 1$. In the limit $\omega_q \to 0$ ($\epsilon \to 0$) we recover the ideal dynamics.

VII. SAW-BASED SPIN-RESONATOR SYSTEM

Here, we provide further details on how to implement experimental candidate systems governed by the class of Hamiltonians given in Eq.(1), using quantum dots embedded in high-quality surface acoustic wave (SAW) resonators [S3, S4]. For similar considerations based on (for example) transmission-line resonators or nanomechanical oscillators, we refer to Refs.[S5] and [S6], respectively.

Charge qubit.—A single electron in a double quantum dot (DQD) coupled to a SAW resonator can be described by

$$H_{\text{charge}} = \frac{\epsilon}{2}\sigma^z + t_c\sigma^x + \omega_c a^\dagger a + g_{\text{ch}}\sigma^z \otimes (a + a^\dagger), \tag{S28}$$

where ϵ is the interdot detuning parameter, t_c the tunnel coupling between the dots, $g_{\text{ch}} = e\phi_0 \mathcal{F}(kd)\sin(kl/2)$ the bare single-phonon coupling strength (assuming a sine-like mode function of the piezoelectric potential, with a node tuned between the two dots separated by a distance l), and the (orbital) Pauli operators are defined as $\sigma^z = |L\rangle\langle L| - |R\rangle\langle R|$ and $\sigma^x = |L\rangle\langle R| + |R\rangle\langle L|$, respectively [S3]. In our expression for g_{ch}, e refers to the electron's charge, and ϕ_0 to the piezoelectric potential associated with a single SAW phonon; the decay of the SAW resonator mode into the bulk is captured by the factor $\mathcal{F}(kd)$, where d is the distance between the DQD and the surface and $k = 2\pi/\lambda_c$ the wavenumber of the resonator mode [S3]. In the computational basis, where the dot Hamiltonian $H_{\text{dot}} = \frac{\epsilon}{2}\sigma^z + t_c\sigma^x$ is diagonal, with the electronic eigenstates

$$|+\rangle = \sin\theta |L\rangle + \cos\theta |R\rangle, \tag{S29}$$
$$|-\rangle = \cos\theta |L\rangle - \sin\theta |R\rangle, \tag{S30}$$

where the mixing angle is given by $\tan\theta = 2t_c/(\epsilon + \Omega)$, $\Omega = \sqrt{\epsilon^2 + 4t_c^2}$, the spin-resonator Hamiltonian given in Eq.(S28) can be rewritten as

$$\begin{aligned} H_{\text{charge}} &= \Omega S^z + \omega_c a^\dagger a + g^x S^x \otimes (a + a^\dagger) \\ &\quad + g^z S^z \otimes (a + a^\dagger), \end{aligned} \tag{S31}$$

where the spin operators in the logical qubit basis are $S^z = (|+\rangle\langle +| - |-\rangle\langle -|)/2$, $S^x = (|+\rangle\langle -| + |-\rangle\langle +|)/2$ and

$$g^x = 4g_{\text{ch}}\sin\theta\cos\theta, \tag{S32}$$
$$g^z = 2g_{\text{ch}}(\cos^2\theta - \sin^2\theta). \tag{S33}$$

Note that in the limit where $\delta, g_{\text{ch}} \ll \omega_c$, with $\delta = \Omega - \omega_c$, one can perform a rotating-wave approximation yielding

the standard Jaynes-Cummings Hamiltonian [S7]. Finally, note that the spin-resonator Hamiltonian given in Eq.(S31) belongs to the general class of Hamiltonians defined in Eq.(1). In particular, at the charge degeneracy point $\epsilon = 0$, where $\sin\theta = \cos\theta = 1/\sqrt{2}$, the Hamiltonian given in Eq.(S31) reduces to

$$H_{\text{charge}} = 2t_c S^z + \omega_c a^\dagger a + 2g_{\text{ch}} S^x \otimes \left(a + a^\dagger\right). \quad (S34)$$

Note that the (pseudo-) spin-resonator coupling is maximized at this charge-degeneracy point, i.e., when there is no bias between the two dots, and decreases as one moves away from this point [S5, S7, S8].

Coupling strength.—Following Ref.[S4], the single phonon coupling strength g_{ch} may be expressed as

$$\frac{g_{\text{ch}}}{\omega_c} = \zeta_{\text{ch}} = \sqrt{\alpha_{\text{eff}}}\sqrt{\frac{l^2\lambda}{V}}, \quad (S35)$$

where V is the mode volume associated with the resonator mode and $\alpha_{\text{eff}} = \alpha K^2 c/v_s \epsilon_r$ is an effective fine-structure constant, defined in terms of the fine structure constant $\alpha \sim 1/137$, the (material-specific) electromechanical coupling coefficient K^2 (as a widely used measure to quantify the piezoelectric coupling strength), the speed of light c, the SAW speed of sound v_s and the relative dielectric constant ϵ_r. The coupling parameter K^2 describes piezoelectric stiffening and may be expressed as $K^2 = e_{14}^2/\underline{c}\epsilon$, where e_{14}, $\underline{c}$, and ϵ refer to representative values of the piezoelectric, the elasticity and the dielectric tensor, respectively. Typical values for $\alpha_{\text{eff}}/\alpha$ range from $\alpha_{\text{eff}}/\alpha \sim 10$ for GaAs up to $\alpha_{\text{eff}}/\alpha \gtrsim 100$ for strongly piezoelectric materials such as LiNbO$_3$ or ZnO, underlining the potential of SAW based systems to reach the ultra-strong coupling regime [S4]. For a typical SAW penetration length $\sim 0.3\lambda$ close to the surface, Eq.(S35) further simplifies to $g_{\text{ch}}/\omega_c \approx (0.5 - 1.5)\sqrt{l^2/A}$, where A refers to the surface mode area. When expressing α_{eff} in terms of the fundamental material parameters, Eq.(S35) can be rewritten as

$$\frac{g_{\text{ch}}}{\omega_c} \approx \frac{e e_{14}}{\epsilon v_s}\sqrt{\frac{1}{\rho v_s}}\sqrt{\frac{l^2\lambda}{V}}. \quad (S36)$$

This estimate also follows from the expression given above, $g_{\text{ch}} = e\phi_0\mathcal{F}(kd)\sin(kl/2)$, with $\phi_0 \approx (e_{14}/\epsilon)\sqrt{\hbar/2\rho V\omega_c}$ [S3], close to the surface $\mathcal{F}(kd) \sim 1$, and with $\sin(kl/2) \approx kl/2$ for $kl/2 \ll 1$ (in the spirit of circuit QED setups).

Spin qubit.—In the two-electron regime of a DQD, one can couple the effective dipole-moment of singlet-triplet subspace to the resonator mode [S3, S9]. Within the two-level subspace (all other levels are far detuned), the dynamics are described by

$$H_{\text{spin}} = \frac{\Omega}{2}\sigma^z + \omega_c a^\dagger a + g^x\sigma^x \otimes \left(a + a^\dagger\right) + g^z\sigma^z \otimes \left(a + a^\dagger\right), \quad (S37)$$

where $\sigma^z = |1\rangle\langle 1| - |0\rangle\langle 0|$, $\sigma^x = |1\rangle\langle 0| + |0\rangle\langle 1|$ and

$$g^x = e\phi_0\mathcal{F}(kd)\,\eta_{\text{geo}}\kappa_0\kappa_1, \quad (S38)$$
$$g^z = e\phi_0\mathcal{F}(kd)\,\eta_{\text{geo}}\left[\kappa_1^2 - \kappa_0^2\right]/2. \quad (S39)$$

Here, $\eta_{\text{geo}} = \sin(kx_R) - \sin(kx_L)$ accounts for the positioning of the DQD with respect to the piezoelectric mode function. The coupling is reduced by the admixtures of the qubit's states $\{|0\rangle, |1\rangle\}$ with the localized singlet $\kappa_n = \langle n|S_{02}\rangle$. Again, for $\Omega \approx \omega_c$ and $g^\alpha \ll \omega_c$, we recover the prototypical Jaynes-Cummings dynamics. Moreover, the spin-resonator Hamiltonian given in Eq.(S37) belongs to the general class of Hamiltonians defined in Eq.(1).

Hot gate.—For such a spin qubit a spin-resonator coupling strength of $g_{\text{sp}}/2\pi \equiv g^x/2\pi = (g_0/2\pi)\kappa_0\kappa_1 \approx 3.2$MHz ($g^z/2\pi \approx 0.64$MHz) has been predicted for typical parameters in GaAs [S3]. For a typical resonator frequency $\omega_c/2\pi \approx 1.5$GHz, this amounts to a relative coupling strength $\mu_{\text{sp}} = g_{\text{sp}}/\omega_c \approx 0.2\%$ and an effective coupling $g_{\text{eff}}/2\pi = \mu_{\text{sp}}g_{\text{sp}}/2\pi \approx 65$kHz, which could be increased substantially by additionally depositing a strongly piezoelectric material such as LiNbO$_3$ or ZnO on the GaAs substrate [S3, S4, S10]. The condition $\omega_c \gg \Omega$ can be satisfied by choosing the magnetic gradient Δ between the dots appropriately, $\Delta \lesssim 0.1\mu$eV. Recently, SAW resonators with quality-factors approaching $\sim 10^6$ have been realized experimentally [S11]. Then, taking an optimistic quality-factor of $Q = 10^6$, according to the hot-gate requirement $k_B T \ll Q \times g_{\text{eff}}$, we find $T \ll 3.1$K; therefore, for spin qubits coupled to high-quality SAW-resonators, our scheme can tolerate temperatures approaching the Kelvin regime, where the thermal occupation number is much larger than one. For example, for $\omega_c/2\pi \approx (1.0 - 1.5)$ GHz and $T \approx 0.5$K, we have $\bar{n}_{\text{th}} \approx 6.5 - 10$. The second requirement for small errors, $\Gamma \ll g_{\text{eff}}$, yields $\Gamma/2\pi \ll 65$kHz, which may be satisfied in GaAs with recently demonstrated echo techniques, where decoherence timescales $T_2 \approx 1$ms have been demonstrated [S12]. Finally, with $\bar{n}_{\text{th}}/Q \approx 10/10^6$ and $\Gamma/\omega_c \approx 1$kHz/1.5GHz, and using the relation $\xi \approx \alpha_\kappa(\kappa/\omega_c)\bar{n}_{\text{th}} + \alpha_\Gamma\Gamma/\omega_c$, we can estimate the overall gate error as $\xi \approx 4 \times 10^{-5} + 2.5 \times 10^{-2} \approx 2.5\%$, which is largely limited by dephasing-induced errors (for the parameters chosen here). Again, to counteract this source of error, a strongly piezoelectric material such as LiNbO$_3$ may be used on the GaAs substrate. Alternatively, one could also investigate silicon quantum dots: while this setup also requires a more sophisticated heterostructure including some piezoelectric layer, it should benefit from prolonged dephasing times $T_2^\star > 100\mu$s [S13], which is not longer than the dephasing time T_2 quoted above for GaAs, but relaxes the need for dynamical decoupling.
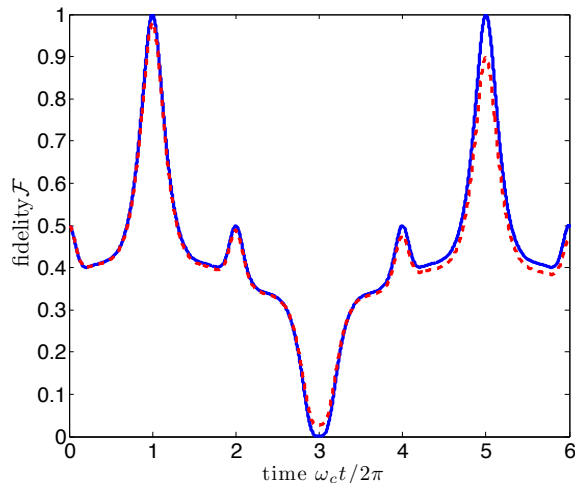
Figure S2: (color online). Fidelity $\mathcal{F}$ for the two-qubit state ρ_{qubits} with the target state $|\Psi_{\text{tar}}\rangle = (|\Uparrow\Downarrow\rangle + i\,|\Downarrow\Uparrow\rangle)/\sqrt{2}$ for $\Gamma/\omega_c = 0$ (blue solid line) and $\Gamma/\omega_c = 1\%$ (red dashed line). For sufficiently low noise, at $\omega_c t = 2\pi$ and $\omega_c t = 5 \times 2\pi$ the fidelity with the maximally entangled state $|\Psi_{\text{tar}}\rangle$ reaches the maximal value $\mathcal{F} = 1$. Numerical parameters: $\omega_q/\omega_c = 0$, $k_B T/\omega_c = 2$ ($\bar{n}_{\text{th}} \approx 1.54$), $g/\omega_c = 1/4$, $\kappa/\omega_c = Q^{-1} = 10^{-5}$.

VIII. ADDITIONAL NUMERICAL RESULTS

Here, we provide further detailed results based on the numerical simulation of the master equation given in Eq.(8). Just as in the main text, for all simulations shown below the initial state of the spin-resonator system has been chosen as $\rho(0) = |\Uparrow\Downarrow\rangle\langle\Uparrow\Downarrow| \otimes \rho_{\text{th}}(T)$, with the cavity mode in the thermal state $\rho_{\text{th}}(T) = Z^{-1}\exp\left[-\beta\omega_c a^\dagger a\right]$.

*Periodic recurrence*s.—First, as displayed in Fig.S2, we observe periodic recurrences of the maximally-entangling dynamics: For example, for $g/\omega_c = 1/4$ (as used in Fig.S2), ideally—apart from $\mathcal{F} = 1$ at $(\omega_c/2\pi)t = 1$—we find $\mathcal{F} = 1$ again at $(\omega_c/2\pi)t = 5$, since $U_{\text{id}}^x(m = 5, 1/4) = \exp\left[i\pi\sigma_1^x\sigma_2^x\right]U_{\text{id}}^x(1, 1/4) = -U_{\text{id}}^x(1, 1/4)$. This statement holds provided that dephasing is negligible on the relevant timescale; compare the dashed curve in Fig.S2 which accounts for dephasing of the qubits.

Non-zero level splitting.—While our analytical treatment has assumed $\omega_q = 0$, in Fig.S3 we provide exemplary numerical results that explicitly account for a non-zero qubit level splitting $\omega_q > 0$, showing that the proposed protocol can tolerate non-zero level splittings of the qubits $\omega_q/\omega_c \lesssim 0.1$, without a severe reduction in the fidelity of the protocol. Again, this numerical finding is corroborated in Fig.S4. Here, it is shown explicitly that a strong entanglement reduction is observed once condition (9) is violated. Conversely, within the range of parameter values satisfying Eq.(9), the results are rather insensitive to the particular parameter values.

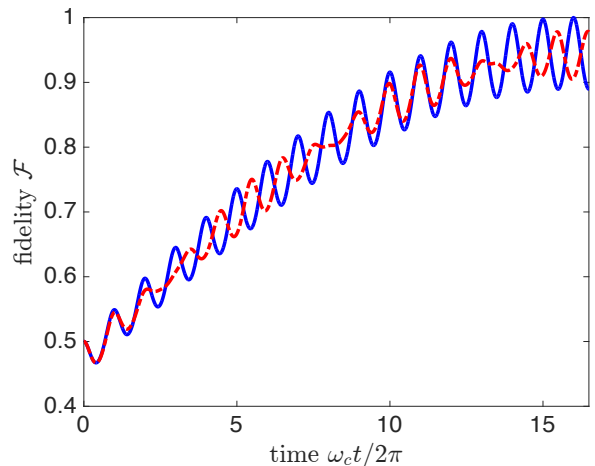*Rethermalization-induced errors*.—As illustrated in

Figure S3: (color online). Fidelity $\mathcal{F} = \langle\Psi_{\text{tar}}|\rho_{\text{qubits}}|\Psi_{\text{tar}}\rangle$ for the two-qubit state $\rho_{\text{qubits}} = \text{Tr}_{\text{cav}}[\rho]$ with the target state $|\Psi_{\text{tar}}\rangle = (|\Uparrow\Downarrow\rangle + i\,|\Downarrow\Uparrow\rangle)/\sqrt{2}$ for both $\omega_q/\omega_c = 0$ (solid blue line) and $\omega_q/\omega_c = 0.1$ (dashed red line); here, $g/\omega_c = 1/16 < 0.1$. Other numerical parameters: $k_B T/\omega_c = 2$ ($\bar{n}_{\text{th}} \approx 1.54$), $Q = 10^5$ and $\Gamma/\omega_c = 0$.
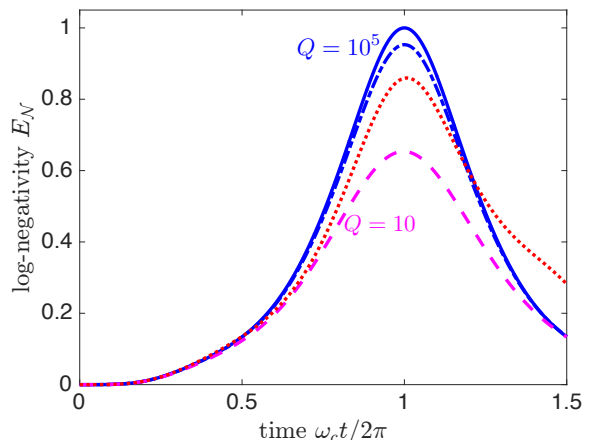

Figure S4: (color online). Logarithmic negativity $E_{\mathcal{N}}$ for $k_B T/\omega_c = 1$ and different cavity quality factors: $Q = 10^5$ (solid blue), $Q = 10^2$ (dash-dotted blue), and $Q = 10$ (dashed magenta). A clear reduction of the maximum entanglement is observed, if the quality factor Q is too low to satisfy the hot-gate requirement given in Eq.(9). Here, we have $g/\omega_c \times g/k_B T = 1/16 = 6.25 \times 10^{-2}$. The red (dotted) curve refers to $Q = 10^2$ and $\omega_q/\omega_c = 0.2$. Other numerical parameters: $g/\omega_c = 1/4$ and $\Gamma/\omega_c = 0$.

Fig.S5, we have numerically checked that (for small infidelities) the rethermalization induced error ξ_κ scales linearly with the effective rethermalization rate $\kappa_{\text{eff}} = \kappa\bar{n}_{\text{th}}$. Notably, as evidenced in Fig.S5, the error is found to be independent of the spin-resonator coupling g. As demonstrated in in Sec. IX, this numerical result can be corroborated analytically within a perturbative framework.

Full error analysis.—Similar to Fig.4(c) in the main text, in Fig.S6 we provide numerical results that fully
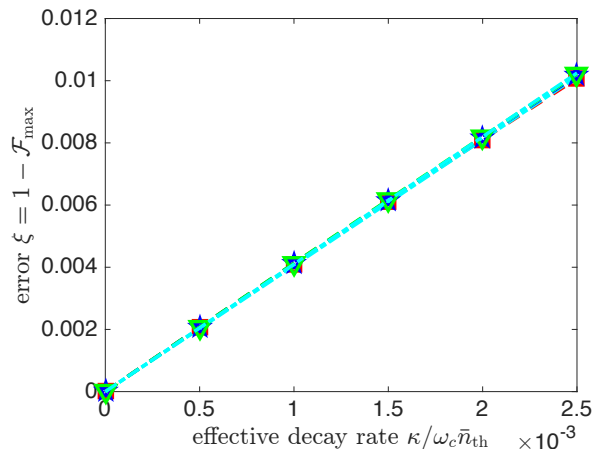
Figure S5: (color online). Error as a function of the effective rethermalization rate $\kappa \bar{n}_{\text{th}}$ for $g/\omega_c = 1/16$ (red squares), $g/\omega_c = 1/(8\sqrt{2})$ (blue stars) and $g/\omega_c = 1/8$ (green triangles) and $k_B T/\omega_c = 2$ ($\bar{n}_{\text{th}} \approx 1.54$), within the relevant small-error regime ($\kappa_{\text{eff}}/g_{\text{eff}} \ll 1$). The dash-dotted lines in cyan refer to linear fits, demonstrating a linear error scaling in the small error-regime ($\kappa_{\text{eff}}/g_{\text{eff}} \ll 1$), which is independent of $\mu = g/\omega_c$. Accordingly, the error is larger for higher temperatures, but all temperature related effects are approximately captured by the thermal occupation number $\bar{n}_{\text{th}}$. Other numerical parameters: $\Gamma = 0$ and $\omega_q = 0$.
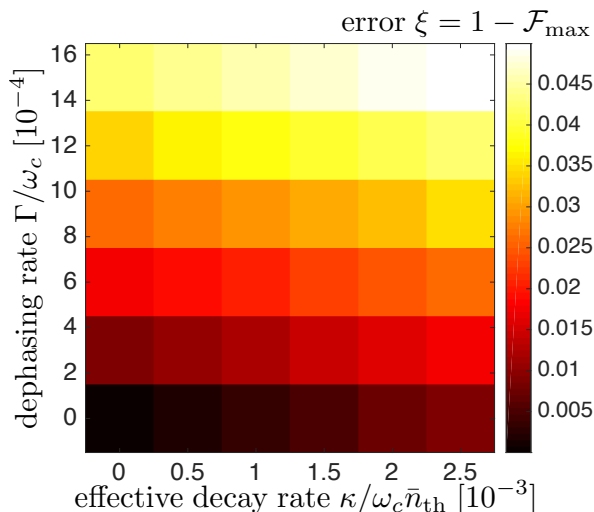

Figure S6: (color online). Total error ξ as a function of both the effective rethermalization rate $\sim \kappa/\omega_c \bar{n}_{\text{th}} \sim \bar{n}_{\text{th}}/Q$ and the spin dephasing rate $\sim \Gamma/\omega_c$ for $g/\omega_c = 1/16$, $k_B T/\omega_c = 4$ and $\omega_q = 0$.

account for higher-order, correlated errors (beyond the linear error approximation). Here, we have chosen a temperature $k_B T/\omega_c = 4$, a factor two larger than the one used in Fig.4(c) in the main text. Still, if the rethermalization induced error is scaled in terms of the effective decay rate $\kappa_{\text{eff}} = \kappa \bar{n}_{\text{th}}$, we obtain (approximately) the same total error ξ, independently of the temperature

$k_B T$, showing that the effective decay rate $\kappa_{\text{eff}} = \kappa \bar{n}_{\text{th}}$ captures well any temperature-related effects. This is evidenced numerically in Fig.S6 which approximately coincides with the results displayed in Fig.4(c) in the main text and is line with our simple error estimate for rethermalization induced errors; compare Eq.(11) in the main text.

Timing errors.—Finally, we consider errors (infidelities) due to limited timing accuracies. To do so, we take the average fidelity of our protocol $\bar{\mathcal{F}}$ within a certain timing window Δt centered around the stroboscopic time t_{max} for which maximum fidelity (minimal infidelity) is achieved; for example, in quantum dot systems timing accuracies Δt of a few picoseconds have been demonstrated experimentally [S14]. For $g/2\pi = 10\text{MHz}$ and $\omega_c/2\pi = 160\text{MHz}$ (that is, $\mu = g/\omega_c = 1/16$) as used in the main text, the pulse time lies in the microsecond regime ($t_{\text{max}} = \pi/8g_{\text{eff}} \approx 0.2\mu s$), for which $\Delta t \approx 1\text{ps}$ is feasible; for this relatively long pulse, the relative time jitter is well below the percent level, i.e., $(\omega_c/2\pi)\Delta t \approx 10^{-4}$. Based on our numerical simulations, we make the following observations: (i) As demonstrated in Fig.S7, we find an average error scaling linearly with $\sim \bar{n}_{\text{th}}$, that is $\bar{\xi} = 1 - \bar{\mathcal{F}} \sim \bar{n}_{\text{th}}$. (ii) More precisely, the error expressions given in the main text can be generalized to

$$\bar{\xi} = \bar{\alpha}_\kappa \frac{\kappa}{\omega_c} \bar{n}_{\text{th}} + \bar{\alpha}_\Gamma \frac{\Gamma}{\omega_c} + \bar{\beta}_\kappa + \bar{\beta}_\Gamma. \qquad (S40)$$

Here, the unit-less quantities $\bar{\alpha}_\gamma, \bar{\beta}_\kappa$ for $\gamma = \kappa, \Gamma$ depend on the timing window Δt. For example, for $g/\omega_c = 1/16$ and $(\omega_c/2\pi)\Delta t = 5\%$, we then extract $\bar{\alpha}_\kappa \approx 4.03$, $\bar{\beta}_\gamma \approx 2.2 \times 10^{-4}$, $\bar{\alpha}_\Gamma \approx 24.22$ and $\bar{\beta}_\Gamma \approx 5.1 \times 10^{-4}$. (iii) As shown in Fig.S7, for the experimentally most relevant regime where $(\omega_c/2\pi)\Delta t \ll 1$ (such that the timing window covers a small range of the oscillations only), this error is found to decrease for a smaller spin-resonator coupling strength g/ω_c, because larger values of g/ω_c imply larger oscillation amplitudes within the relevant range over which we have to average; compare the center and right plots in Fig.S7. Therefore, for the experimentally most relevant regime where $(\omega_c/2\pi)\Delta t \ll 1$ and $g/\omega_c \lesssim 1/16$, the effects of time jitter should be negligible.

IX. ANALYTICAL EXPRESSION FOR RETHERMALIZATION-INDUCED ERRORS

In this Appendix we derive an analytical expression for rethermalization-induced errors. In particular we show that this expression is independent of the spin-resonator coupling strength g.

Our analysis starts out from the master equation

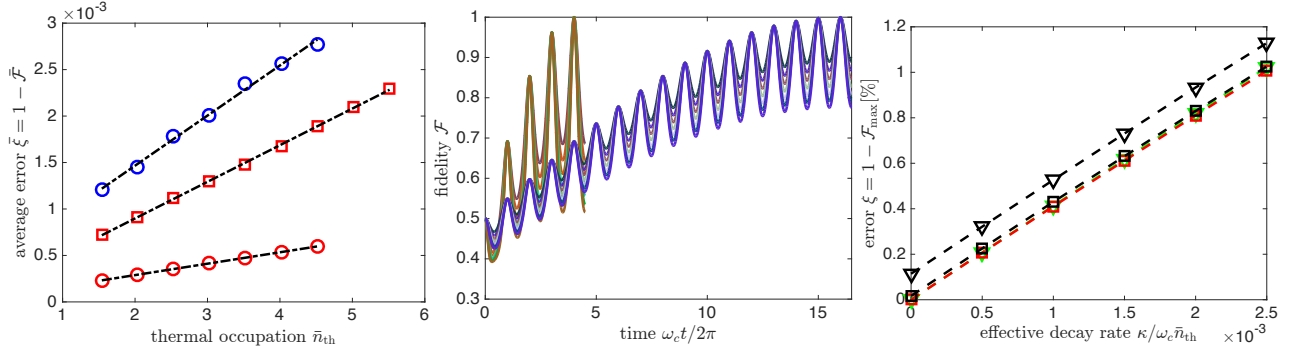$$\dot{\rho} = -i[H, \rho] + \sum_{j=1,2} \mathcal{D}[L_j]\rho, \qquad (S41)$$

Figure S7: (color online). Timing errors. Left: Total average error $\bar{\xi}$ as a function of the thermal occupation number $\bar{n}_{\text{th}}$ for timing windows $(\omega_c/2\pi)\,\Delta t = 5\%$ (circles) and $(\omega_c/2\pi)\,\Delta t = 10\%$ (squares); here, $g/\omega_c = 1/16$ (red symbols) and $g/\omega_c = 1/8$ (blue symbols, upper curve). All curves can be fit very well to linear error models (see black dashed lines). Center: Set of underlying (temperature-dependent) simulations for both $g/\omega_c = 1/16$ (terminating at $\omega_c t/2\pi = 16.5$) and $g/\omega_c = 1/8$ (terminating at $\omega_c t/2\pi = 4.5$). Note that larger amplitudes are observed for larger values of $\mu = g/\omega_c$. Other numerical parameters: $Q = 10^5$, $\Gamma = 0$ and $\omega_q = 0$. Right: Same analysis as done in Fig.S5 for $g/\omega_c = 1/8$ (triangles) and $g/\omega_c = 1/16$ (squares). The black curves account for a finite timing accuracy $(\omega_c/2\pi)\,\Delta t = 5\%$, showing that the detrimental effects of time jitter are less pronounced for smaller values of $\mu = g/\omega_c$.

where the Hamiltonian $H = \omega_c a^\dagger a + g\mathcal{S} \otimes (a + a^\dagger)$ refers to the ideal (noise-free) dynamics and the jump-operators $L_1 = \sqrt{\kappa_1}a$, $L_2 = \sqrt{\kappa_2}a^\dagger$ with $\kappa_1 = \kappa\,(\bar{n}_{\text{th}} + 1)$ and $\kappa_2 = \kappa\bar{n}_{\text{th}}$ describe rethermalization of the resonator mode with a rate $\kappa = \omega_c/Q$ that is enhanced by the thermal occupation number $\bar{n}_{\text{th}}$. It is convenient to move to an interaction picture, defined by $\tilde{\rho}(t) = \exp[iHt]\,\rho(t)\,\exp[-iHt]$. In this interaction picture, the system's dynamics is described by

$$\dot{\tilde{\rho}} = \sum_{j=1,2} \mathcal{D}\left[\tilde{L}_j\right]\tilde{\rho}, \qquad (S42)$$

with time-dependent jump operators $\tilde{L}_j = \exp[iHt]\,L_j\,\exp[-iHt]$. Using the exact relation $\exp[-iHt] = U\exp[-i\omega_c ta^\dagger a]\,U^\dagger U_{\text{sp}}(t)$, with the polaron transformation $U = \exp[\mu\mathcal{S}(a - a^\dagger)]$ and the pure spin (entangling) gate $U_{\text{sp}}(t) = \exp[i\mu^2\omega_c t\mathcal{S}^2]$, the time-dependent jump operators $\tilde{L}_j$ take on a simple form

$$\tilde{L}_1(\tau) = \sqrt{\kappa_1}\left[e^{-i\omega_c\tau}a + (e^{-i\omega_c\tau} - 1)\mu\mathcal{S}\right],$$
$$\tilde{L}_2(\tau) = \sqrt{\kappa_2}\left[e^{i\omega_c\tau}a^\dagger + (e^{i\omega_c\tau} - 1)\mu\mathcal{S}\right]. \qquad (S43)$$

The formal solution to Eq.(S42) reads

$$\tilde{\rho}(t) = \tilde{\rho}(0) + \sum_j \int_0^t d\tau \mathcal{D}\left[\tilde{L}_j(\tau)\right]\tilde{\rho}(\tau), \qquad (S44)$$

where in the interaction picture the zeroth-order solution $\tilde{\rho}_0(t) = \tilde{\rho}(0) = \rho(0)$ stays inert, and accounts for the ideal (noise-free) dynamics only in the lab frame, $\rho_0(t) = \exp[-iHt]\,\tilde{\rho}_0(t)\,\exp[iHt] = \exp[-iHt]\,\rho(0)\,\exp[iHt]$. To obtain the first-order correction $\tilde{\rho}_1(t)$ within a perturbative framework, we re-insert the zeroth-order solution into the dissipator of Eq.(S44), i.e. effectively we take $\tilde{\rho}(\tau) \to \rho(0)$, which yields $\tilde{\rho}(t) \approx \rho(0) + \tilde{\rho}_1(t)$, with

$$\tilde{\rho}_1(t) = \sum_j \int_0^t d\tau \mathcal{D}\left[\tilde{L}_j(\tau)\right]\rho(0). \qquad (S45)$$

Inserting the expressions given in Eq.(S43) into Eq.(S45) and performing the integration, with $\int_0^t d\tau\,\left|1 - e^{\pm i\omega_c\tau}\right|^2 = 2(t - \frac{\sin(\omega_c t)}{\omega_c})$ and $\int_0^t d\tau\,(1 - e^{\pm i\omega_c\tau}) = t \pm i\frac{e^{\pm i\omega_c t} - 1}{\omega_c}$, one arrives at

$$\tilde{\rho}_1(t) = \kappa_1 t\mathcal{D}[a]\rho(0) + \kappa_2 t\mathcal{D}[a^\dagger]\rho(0) + 2(\kappa_1 + \kappa_2)\mu^2\left(t - \frac{\sin(\omega_c t)}{\omega_c}\right)\mathcal{D}[\mathcal{S}]\rho(0)$$

$$+ \left[\kappa_1\mu\left(t - i\frac{e^{-i\omega_c t} - 1}{\omega_c}\right)\left\{a\rho(0)\mathcal{S} - \frac{1}{2}\{a\mathcal{S}, \rho(0)\}\right\} + \text{h.c.}\right]$$

$$+ \left[\kappa_2\mu\left(t + i\frac{e^{i\omega_c t} - 1}{\omega_c}\right)\left\{a^\dagger\rho(0)\mathcal{S} - \frac{1}{2}\{a^\dagger\mathcal{S}, \rho(0)\}\right\} + \text{h.c.}\right]. \qquad (S46)$$

which, for stroboscopic times $t_m = 2\pi m/\omega_c$ (with m integer), simplifies to

$$\tilde{\rho}_1(t_m) = \kappa_1 t_m \mathcal{D}[a]\rho(0) + \kappa_2 t_m \mathcal{D}[a^\dagger]\rho(0) + 2(\kappa_1 + \kappa_2)\mu^2 t_m \mathcal{D}[\mathcal{S}]\rho(0)$$
$$+ \left[\kappa_1 \mu t_m \left\{a\rho(0)\mathcal{S} - \frac{1}{2}\{a\mathcal{S}, \rho(0)\}\right\} + \text{h.c.}\right] + \left[\kappa_2 \mu t_m \left\{a^\dagger \rho(0)\mathcal{S} - \frac{1}{2}\{a^\dagger \mathcal{S}, \rho(0)\}\right\} + \text{h.c.}\right].$$

Next, we perform a transformation back to the lab frame, with $\rho(t) = \exp[-iHt]\tilde{\rho}(t)\exp[iHt]$. As discussed in the main text, for stroboscopic times the ideal evolution simplifies to $\exp[-iHt_m] = \exp[i\mu^2 2\pi m \mathcal{S}^2] = \exp(-i\phi_{\text{gp}})\exp[i4\pi m\mu^2\sigma_1^x\sigma_2^x]$. The ideal (noise-free) evolution is given by $\rho_{\text{id}}(t_m) = \exp[-iHt_m]\rho(0)\exp[iHt_m] = \varrho_{\text{id}}(t_m)\otimes\rho_{\text{th}}$, where $\varrho_{\text{id}}(t_m) = \exp[i4\pi m\mu^2\sigma_1^x\sigma_2^x]\varrho(0)\exp[-i4\pi m\mu^2\sigma_1^x\sigma_2^x]$ is the ideal qubit's state at time t_m, starting from the initial state $\rho(0) = \varrho(0)\otimes\rho_{\text{th}}$. Then, the system's density matrix at time t_m is approximately given by

$$\rho(t_m) = \rho_{\text{id}}(t_m) + \kappa_1 t_m \mathcal{D}[a]\rho_{\text{id}}(t_m)$$
$$+ \kappa_2 t_m \mathcal{D}[a^\dagger]\rho_{\text{id}}(t_m)$$
$$+ 2(\kappa_1 + \kappa_2)\mu^2 t_m \mathcal{D}[\mathcal{S}]\rho_{\text{id}}(t_m)$$
$$+ \left[\kappa_1 \mu t_m \left\{a\rho_{\text{id}}(t_m)\mathcal{S} - \frac{1}{2}\{a\mathcal{S}, \rho_{\text{id}}(t_m)\}\right\}\right.$$
$$\left. + \kappa_2 \mu t_m \left\{a^\dagger \rho(0)\mathcal{S} - \frac{1}{2}\{a^\dagger \mathcal{S}, \rho(0)\}\right\} + \text{h.c.}\right].$$

Note that, in the limit $\kappa_i \to 0$, one retrieves the ideal result $\rho(t_m) = \rho_{\text{id}}(t_m)$. Next, we trace out the resonator mode. Assuming the state of the resonator mode to be diagonal in the occupation number basis (in particular, this holds for a thermal state ρ_{th}), none of the cross-terms contribute to the partial trace, and for stroboscopic times t_m the state of the qubits is given by

$$\varrho(t_m) = \varrho_{\text{id}}(t_m) + 2\kappa(2\bar{n}_{\text{th}} + 1)t_m\mu^2\mathcal{D}[\mathcal{S}]\varrho_{\text{id}}(t_m). \tag{S47}$$

As expected naïvely, the error term scales with $\sim \kappa\bar{n}_{\text{th}}t_m$, but is is further reduced by the factor $\mu^2 = (g/\omega_c)^2$. Eq.(S47) holds for stroboscopic times $t_m = 2\pi m/\omega_c$, with m integer. If $m\mu^2 = 1/16$, the ideal evolution $\exp[-iHt_m] = \exp(-i\phi_{\text{gp}})\exp[i\frac{\pi}{4}\sigma_1^x\sigma_2^x]$ equals a maximally-entangling gate, which (for an initial pure state like $|\Psi\rangle_0 = |\Downarrow\Downarrow\rangle$) yields the desired ideal qubit target state $|\Psi_{\text{tar}}\rangle = \exp[i\frac{\pi}{4}\sigma_1^x\sigma_2^x]|\Psi\rangle_0$. Then, in the presence of noise, at the nominally ideal time $t_{\text{max}} = \pi/8\mu^2\omega_c = \pi/8g_{\text{eff}}$ the qubit's density matrix reads

$$\varrho(t_{\text{max}}) = |\Psi_{\text{tar}}\rangle\langle\Psi_{\text{tar}}| \tag{S48}$$
$$+ \frac{\pi}{4}\frac{\kappa}{\omega_c}(2\bar{n}_{\text{th}} + 1)\mathcal{D}[\mathcal{S}]|\Psi_{\text{tar}}\rangle\langle\Psi_{\text{tar}}|.$$

Therefore, to first order rethermalization-induced noise leads to dephasing dynamics in the eigenbasis of $\mathcal{S}$ with a single such phase flip. Since neither the desired target state $|\Psi_{\text{tar}}\rangle$ not the initial state $|\Psi\rangle_0$ is an eigenstate of $\mathcal{S}$, the system looses fidelity with a probability
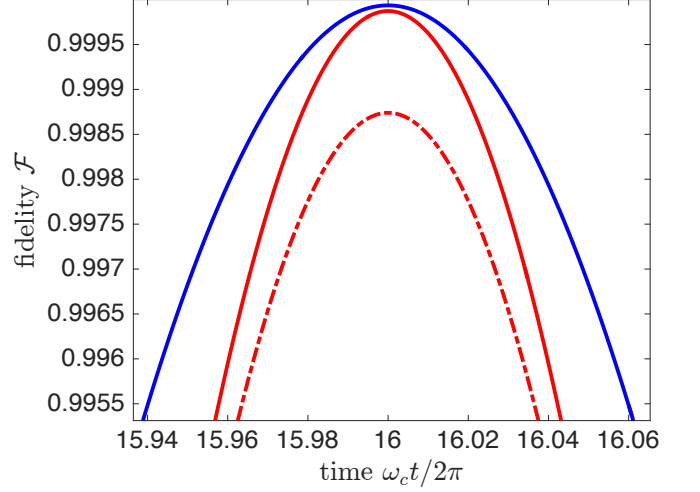

Figure S8: (color online). Fidelity $\mathcal{F}$ close to the ideal time t_{max} for $g/\omega_c = 1/16$. The different curves refer to $Q = 10^5$, $k_B T/\omega_c = 2$, i.e. $\bar{n}_{\text{th}} \approx 1.54$, (blue solid, top curve), $Q = 10^5$, $k_B T/\omega_c = 4$, i.e. $\bar{n}_{\text{th}} \approx 3.52$, (red solid) and $Q = 10^4$, $k_B T/\omega_c = 4$ (red dash-dotted). The error $\xi = 1 - \mathcal{F}$ can be estimated well with the formula $\xi_\kappa \approx 4\bar{n}_{\text{th}}/Q$, giving (for example) $\mathcal{F} \approx 1 - 4 \times 3.52/10^4 \approx 0.9986$. Other numerical parameters: $\Gamma = 0$ and $\omega_q = 0$.

$\frac{\pi}{4}\frac{\kappa}{\omega_c}(2\bar{n}_{\text{th}} + 1)$; notably, this expression is independent of the spin-resonator coupling strength g.

For the fidelity with the maximally entangled target state, we then obtain

$$\mathcal{F} = \langle\Psi_{\text{tar}}|\varrho(t_{\text{max}})|\Psi_{\text{tar}}\rangle = 1 - \frac{\pi}{2}\frac{\kappa}{\omega_c}(2\bar{n}_{\text{th}} + 1), \tag{S49}$$

with a thermalization-induced error term given by

$$\xi_\kappa = \pi(\kappa/\omega_c)\bar{n}_{\text{th}} + \frac{\pi}{2}Q^{-1}. \tag{S50}$$

This analytical result is in good agreement with our numerical findings (from which we have deduced $\xi_\kappa \approx \alpha_\kappa(\kappa/\omega_c)\bar{n}_{\text{th}}$, with $\alpha_\kappa \approx 4$), showing (i) a linear scaling with the effective rethermalization rate $\sim \kappa\bar{n}_{\text{th}}$, (ii) with a pre-factor $\alpha_\kappa = \pi$ (close to ~ 4) that is *independent* of the spin-resonator coupling strength g and (iii) a constant offset $\sim Q^{-1}$ which is negligible for realistic quality factors $Q \approx 10^5 - 10^6$. The latter is due to photon/phonon emission with a rate $\sim \kappa = \omega_c/Q$ at $T \to 0$. As illustrated further in Fig.S8 with a close-up of the fidelity $\mathcal{F}(t)$ around the optimal point t_{max}, the error ξ_κ can be estimated well with this simple formula, where all

temperature related effects are captured by the simple linear expression in the thermal occupation number $\bar{n}_{\text{th}}$.

X. ANALYTICAL MODEL FOR DEPHASING-INDUCED ERRORS

In this Appendix we provide an analytical model for dephasing-induced errors. Neglecting rethermalization-induced errors for the moment, here we consider the following master equation

$$\dot{\rho} = \underbrace{-i\left[H_{\text{id}}, \rho\right]}_{\mathcal{L}_0 \rho} + \underbrace{\gamma_\phi \left[\mathcal{D}\left[\sigma_1^z\right]\rho + \mathcal{D}\left[\sigma_2^z\right]\rho\right]}_{\mathcal{L}_1 \rho}, \quad \text{(S51)}$$

where $H_{\text{id}} = \omega_c a^\dagger a + g\left(\sigma_1^z + \sigma_2^z\right) \otimes \left(a + a^\dagger\right)$ describes the ideal (error-free), coherent evolution for longitudinal coupling between the qubits and the resonator mode, and γ_ϕ is the pure dephasing rate. Since the superoperators $\mathcal{L}_0$ and $\mathcal{L}_1$ as defined in Eq.(S51) commute, that is $[\mathcal{L}_0, \mathcal{L}_1] = 0$ (since $[H_{\text{id}}, \mathcal{D}\left[\sigma_i^z\right] X] = \mathcal{D}\left[\sigma_i^z\right][H_{\text{id}}, X]$ for any operator X), the full evolution simplifies to

$$\rho(t) = e^{\mathcal{L}_1 t}e^{\mathcal{L}_0 t}\rho(0) = e^{\mathcal{L}_1 t}\rho_{\text{id}}(t), \quad \text{(S52)}$$

where we have defined the ideal target state at time t as $\rho_{\text{id}}(t) = \exp\left[\mathcal{L}_0 t\right]\rho(0)$, which, starting from the initial state $\rho(0)$, exclusively accounts for the ideal (error-free), coherent evolution. For small infidelities ($\gamma_\phi t \ll 1$), the deviation from the ideal dynamics $\Delta\rho = \rho - \rho_{\text{id}}$ is approximately given by

$$\Delta\rho(t) \approx \gamma_\phi t \sum_i \mathcal{D}\left[\sigma_i^z\right]\rho_{\text{id}}(t), \quad \text{(S53)}$$

showing that (in the regime of interest where $\gamma_\phi t \ll 1$) the dominant dephasing induced errors are linearly proportional to $\sim \gamma_\phi t_g \sim \gamma_\phi/g_{\text{eff}} = \gamma_\phi/\mu^2\omega_c$, as expected; here, $t_g \sim g_{\text{eff}}$ is the relevant gate time which has to be short compared to γ_ϕ^{-1}.

In what follows, for completeness we derive the same result within a quantum jump approach. Eq.(S51) can be rewritten as

$$\dot{\rho} = -iH\rho + i\rho H^\dagger + \mathcal{J}\rho, \quad \text{(S54)}$$

where $H = H_{\text{id}} - i\gamma_\phi$ and $\mathcal{J}\rho = \gamma_\phi \sum_i \sigma_i^z \rho \sigma_i^z$. The formal solution to Eq.(S54) reads

$$\rho(t) = e^{-iHt}\rho(0)e^{iH^\dagger t} + \int_0^t d\tau e^{-iH(t-\tau)}\mathcal{J}\rho(\tau)e^{iH^\dagger(t-\tau)}. \quad \text{(S55)}$$

Defining the ideal target state at time t as

$$\rho_{\text{id}}(t) = e^{-iH_{\text{id}}(t-\tau)}\rho(\tau)e^{iH_{\text{id}}(t-\tau)}, \quad \text{(S56)}$$

the exact solution given in Eq.(S55) can be iterated, giving an illustrative expansion in terms of the jumps $\mathcal{J}$. It

reads

$$\rho(t) = \mathcal{U}(t)\rho(0) + \int_0^t d\tau_1 \mathcal{U}(t - \tau_1)\mathcal{J}\mathcal{U}(\tau_1)\rho(0)$$
$$+ \int_0^t d\tau_2 \int_0^{\tau_2} d\tau_1 \mathcal{U}(t - \tau_2)\mathcal{J}\mathcal{U}(\tau_2 - \tau_1) \times$$
$$\mathcal{J}\mathcal{U}(\tau_1)\rho(0) + \dots$$

Here, the n-th order term comprises n jumps $\mathcal{J}$ with free evolution $\mathcal{U}(t)\rho = e^{-iHt}\rho e^{iH^\dagger t}$ between the jumps. Up to second order in $\mathcal{J}$ we then find

$$\rho(t) = \mathcal{U}(t)\rho(0) + e^{-2\gamma_\phi t}\gamma_\phi t \sum_i \sigma_i^z \rho_{\text{id}}(t)\sigma_i^z \quad \text{(S57)}$$
$$+ \frac{1}{2}e^{-2\gamma_\phi t}\gamma_\phi^2 t^2 \sum_{i,j} \sigma_i^z \sigma_j^z \rho_{\text{id}}(t)\sigma_j^z \sigma_i^z + \dots$$

For the regime of interest where $\gamma_\phi t \ll 1$, we then obtain again the result given in Eq.(S53), where the dominant error term scales linearly with $\sim \gamma_\phi t$.

XI. AVERAGE GATE FIDELITY

The average gate fidelity $\bar{F}$ is a useful measure in order to quantify how well the completely-positive, trace-preserving quantum operation $\mathcal{M}$ (in the presence of noise) approximates a given unitary gate U_{id}, which represents the ideal (noise-free) evolution. Formally, it is defined as

$$\bar{F} = \int d\psi \langle\psi| U_{\text{id}}^\dagger \mathcal{M}\left(|\psi\rangle\langle\psi|\right) U_{\text{id}} |\psi\rangle, \quad \text{(S58)}$$

where the integral runs over the uniform (Haar) measure $d\psi$ on state space, with $\int d\psi = 1$ [S15]. As shown in Ref.[S15], $\bar{F}$ may be re-expressed as

$$\bar{F} = \frac{dF_{\text{ent}} + 1}{d + 1}, \quad \text{(S59)}$$

where d is the dimension of the Hilbert space ($d = 4$ for two qubits) and the entanglement fidelity F_{ent} is the fidelity of the state obtained when $\mathcal{M}$ acts on one half of a maximally entangled state with the state obtained from the action of the ideal evolution; it is given by

$$F_{\text{ent}} = \frac{1}{d^3} \sum_{P \in G} \text{tr}\left[P^\dagger U_{\text{id}}^\dagger \mathcal{M}(P) U_{\text{id}}\right]. \quad \text{(S60)}$$

Here, G is a set of $d \times d$ unitary operators, forming a basis for a qudit, i.e., $\text{tr}\left[P_j^\dagger P_k\right] = \delta_{jk}d$, $j, k = 1, \dots, d^2$. For two qubits we may take the set of Pauli matrices modulo phase, comprising in total 16 operators $G = \left\{\mathbb{1}, \sigma_i^\alpha, \sigma_1^\alpha \sigma_2^\beta\right\}$, with $i = 1, 2$, $\alpha = x, y, z$. Experimentally, $\bar{F}$ may be determined using standard state tomography [S15].
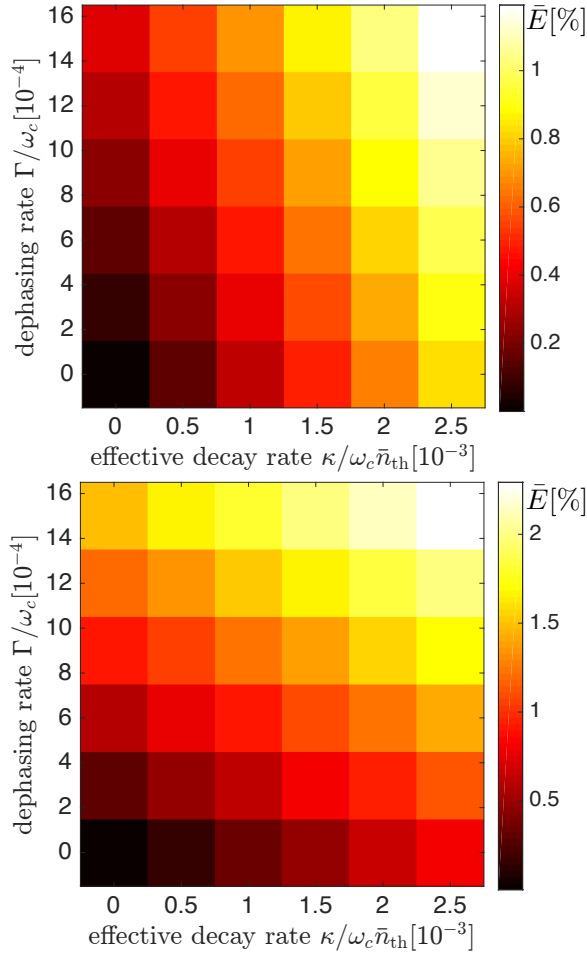
Figure S9: (color online). Total average gate error $\bar{E}$ (in percent) as a function of both the effective rethermalization rate $\sim \kappa/\omega_c \bar{n}_{\text{th}} \sim \bar{n}_{\text{th}}/Q$ and the spin dephasing rate $\sim \Gamma/\omega_c$ for $g/\omega_c = 1/4$ (top) and $g/\omega_c = 1/8$ (bottom). Other numerical parameters: $k_B T/\omega_c = 2$ and $\omega_q = 0$.

Errors.—The average gate error (infidelity) is defined as $\bar{E} = 1 - \bar{F}$. As follows directly from Eq.(S59), it is related to the entanglement infidelity $E_{\text{ent}} = 1 - F_{\text{ent}}$ via $\bar{E} = d/(d+1) \times E_{\text{ent}}$; thus, for two qubits $\bar{E} = (4/5) E_{\text{ent}}$.

Numerical results.—Numerical results for the average gate error $\bar{E}$ are presented in Fig.S9. Here, the map $\mathcal{M}(P)$ is given implicitly as $\mathcal{M}(P) = \text{tr}_a \left[e^{\mathcal{L} t_{\max}} P \otimes \rho_{\text{th}} \right]$, where the superoperator $\mathcal{L}\bullet = -i[H, \bullet] + \mathcal{L}_{\text{noise}}\bullet$ is the Liouvillian associated with the master equation given in Eq.(8) in the main text, which includes undesired processes due to rethermalization of the cavity mode and dephasing of the spins. Broadly speaking, our numerical results for the (average) gate error $\bar{E}$ are comparable to the ones obtained for the state infidelity $\xi = 1 - \mathcal{F}$, as discussed in the main text. First, comparison of our results for $g/\omega_c = 1/4$ and $g/\omega_c = 1/8$ shows that rethermalization-induced errors are approximately independent of the spin-resonator coupling g; for example, for $\Gamma = 0$ and $\kappa/\omega_c \bar{n}_{\text{th}} = 2.5 \times 10^{-3}$ we find $\bar{E}_\kappa \approx 0.82\%$ for both $g/\omega_c = 1/4$ and $g/\omega_c = 1/8$, respectively. Second, as expected, the dephasing induced error scales as $\bar{E}_\Gamma \sim 1/g^2 \sim 1/\mu^2$; for example, as shown in Fig.S9, for $\kappa = 0$ and $\Gamma/\omega_c = 1.5 \times 10^{-3}$, we find $\bar{E}_\Gamma \approx 0.376\%$ and $\bar{E}_\Gamma \approx 1.49\% \approx 4 \times 0.376\%$ for $g/\omega_c = 1/4$ and $g/\omega_c = 1/8$, respectively.

[S1] A. Blais, R.-S. Huang, A. Wallraff, S. M. Girvin, and R. J. Schoelkopf, Phys. Rev. A **69**, 062320 (2004).
[S2] M. Trif, V. N. Golovach, and D. Loss, Phys. Rev. B **77**, 045434 (2008).
[S3] M. J. A. Schuetz, E. M. Kessler, G. Giedke, L. M. K. Vandersypen, M. D. Lukin, and J. I. Cirac, Phys. Rev. X **5**, 031031 (2015).
[S4] J. C. Chen, Y. Sato, R. Kosaka, M. Hashisaka, K. Muraki, and T. Fujisawa, Sci. Rep. **5**, 15176 (2015).
[S5] X. Hu, Y.-x. Liu, and F. Nori, Phys. Rev. B **86**, 035314 (2012).
[S6] P. Rabl, S. J. Kolkowitz, F. H. L. Koppens, J. G. E. Harris, P. Zoller, and M. D. Lukin, Nat. Phys. **6**, 602 (2010).
[S7] T. Frey, P. J. Leek, M. Beck, A. Blais, T. Ihn, K. Ensslin, and A. Wallraff, Phys. Rev. Lett. **108**, 046807 (2012).
[S8] P.-Q. Jin, M. Marthaler, J. H. Cole, A. Shnirman, and G. Schön, Phys. Rev. B **84**, 035322 (2011).
[S9] J. M. Taylor and M. D. Lukin, arXiv:cond-mat/0605144.
[S10] M. V. Gustafsson, P. V. Santos, G. Johansson, and P. Delsing, Nat. Phys. **8**, 338 (2012).
[S11] R. Manenti, M. J. Peterer, A. Nersisyan, E. B. Magnusson, A. Patterson, and P. L. Leek, Phys. Rev. B **93**, 041411(R) (2016).
[S12] F. K. Malinowski *et al.*, arXiv:1601.06677 (unpublished).
[S13] M. Veldhorst et al., Nat. Nanotechnol. **9**, 981 (2014).
[S14] E. Bocquillon *et al.*, Science **339**, 1054 (2013).
[S15] M. A. Nielsen, Phys. Lett. A **303**, 249 (2002).